doi:10.1016/j.ymthe.2005.08.009

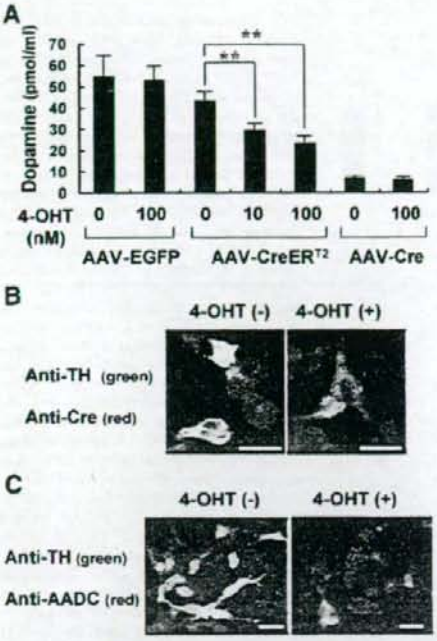

FIG. 2. Reduced dopamine synthesis after 4-OHT-induced ablation of a floxed TH transgene. HEK293 cells were infected with dopamine-synthesizing vectors (AAV-floxed TH, AAV-AADC, and AAV-GCH) in combination with AAV-CreER^{T2} or control vectors. (A) Dopamine content in the culture medium was significantly reduced in the presence of 4-OHT. $^{**}P < 0.01$, $n = 4$. (B) TH (green) and CreER^{T2} (red) immunocytochemistry was performed 48 h after vector infection. Yellow fluorescence in the merged image indicates colocalization. In the presence of 4-OHT, CreER^{T2} translocated to the nucleus. TH was not expressed in cells positive for nuclear CreER^{T2}. Bar, 20 μm. (C) TH (green) and AADC (red) immunocytochemistry. Note the reduced number of TH-positive cells in the presence of 4-OHT. Bar, 20 μm.

with AAV-CreER^{T2} or control vectors. We found that treatment with 4-OHT significantly reduced dopamine synthesis (Fig. 2A). Immunocytochemistry demonstrated coexpression of TH and CreER^{T2} in the cytoplasm in the absence of 4-OHT and an absence of TH expression when CreER^{T2} was translocated into the nucleus in the presence of 4-OHT (Fig. 2B). The expression of AADC was not reduced by the presence of 4-OHT (Fig. 2C). Dual labeling showed that more than 80% of the TH-immunoreactive (TH-IR) cells were also positive for AADC (251 of 300) and Cre (242 of 300) in the absence of 4-OHT-treatment.

Reduction of Dopamine Production in a Rat Model

We next tested whether the vector-mediated Cre-dependent regulation of transgene expression observed in culture could be extended to animal models. We obtained hemiparkinsonian rats by injecting a selective neurotoxin, 6-hydroxydopamine (6-OHDA), into the left medial forebrain bundle. The animals then received a mixture of AAV-CreER^{T2}, AAV-floxed TH, AAV-AADC, and AAV-GCH into their lesioned striatum, after which two-thirds were further treated with 4-OHT (4 mg/kg by intraperitoneal injection for 5 days) during the course of experimentation. Control rats were injected with AAV-LacZ alone or with AAV-Cre plus AAV-floxed TH, AAV-AADC, and AAV-GCH. To evaluate abnormal motor functions associated with depletion of dopamine in the striatum, we repeated quantification of apomorphine-induced rotation, as well

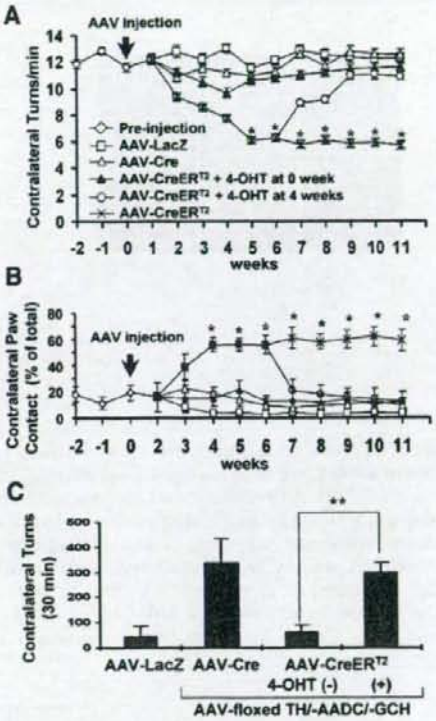

FIG. 3. Temporal control of dopamine synthesis in a rat model of PD transduced with AAV vectors. Sixty hemiparkinsonian rats were generated by 6-OHDA injection. Thirty-six received a mixture of AAV-CreER^{T2}, AAV-floxed TH, AAV-AADC, and AAV-GCH, after which they were divided into three groups of 12. Two of the groups were treated with 4-OHT (4 mg/kg by intraperitoneal injection for 5 days), at the same time or 4 weeks after vector injection. Control PD rats were injected with AAV-LacZ alone ($n = 12$) or AAV-Cre ($n = 12$), instead of AAV-CreER^{T2} with AAV-floxed TH, AAV-AADC, and AAV-GCH. (A) The total number of complete body turns induced by apomorphine was counted for each rat, and (B) spontaneous limb use was scored using the cylinder test. $^{*}P < 0.05$. (C) Efficient conversion of L-dopa to dopamine by AADC. L-Dopa (5 mg/kg) was administered to 4-OHT-treated rats and AAV-Cre-injected rats. Contralateral turning in response to L-dopa was counted for 30 min. $^{**}P < 0.01$. Legend symbols are as shown in A and B.

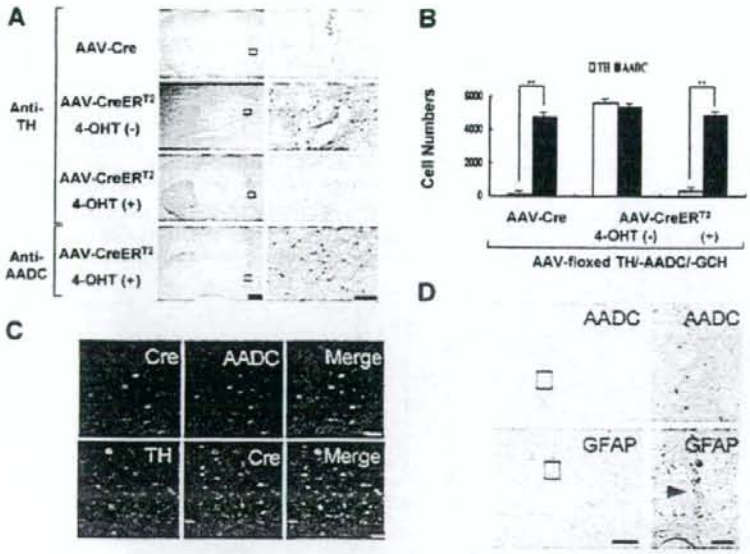

FIG. 4. Selective ablation of the TH transgene induced by treatment with 4-OHT. (A) Immunohistochemical staining for TH or AADC in the brains of 6-OHDA-lesioned rats 12 weeks after stereotaxic injection of AAV-Cre or AAV-CreER^{T2}, with or without 4-OHT treatment. AAV vectors were injected into the lesioned side of the striatum (right side of the photos). High-power-magnified images of the vector injection sites (squares in the left column) are shown in the right column. Representative photographs are also shown. Bar, 1.5 mm (left column), 100 μm (right column). (B) Number of immunoreactive (IR) cells against TH or AADC in the multiple AAV vector-injected striatum. The number of cells in 11 sections per rat ($n = 3$ for each group) was counted. The numbers of TH-IR cells and AADC-IR cells in AAV-CreER^{T2}-injected rats given 4-OHT 0 or 4 weeks after vector injection were indistinguishable and the results pooled for comparison with other groups. $^{**}P < 0.01$. (C) Efficient cotransduction of AAV vectors, as determined by dual immunofluorescence staining of the 6-OHDA-lesioned striatum. The majority of Cre-IR cells were also positive for TH and AADC. Bar, 20 μm. (D) Parallel striatal sections immunostained for glial fibrillary acidic protein (GFAP) or AADC. Striatal cells were transduced without obvious reactive astrocytosis. Residual hemosiderin was observed along the needle tract. On the right are magnified views of the boxes on the left. Bars: 0.5 mm, left; 50 μm, right.

as the cylinder test, weekly until the rats were killed. In the absence of 4-OHT, we observed behavioral recovery in rats that received both AAV-CreER^{T2} and AAV vectors expressing dopamine-synthesizing enzymes. Following 4-OHT treatment, these rats regressed, demonstrating impaired behavior (Figs. 3A and 3B). No recovery occurred in AAV-CreER^{T2}-injected rats treated with 4-OHT at the same time as vector injection or in AAV-Cre- or AAV-LacZ-injected rats. Contralateral turning in response to L-3,4-dihydroxyphenylalanine (L-dopa, 5 mg/kg) was not significantly reduced in 4-OHT-treated rats or AAV-Cre injected rats, indicating efficient conversion of L-dopa to dopamine in the striatum due to preservation of AADC activity (Fig. 3C).

Immunohistochemistry showed fewer TH-IR cells in rats that received AAV-Cre or AAV-CreER^{T2} plus 4-OHT, compared to injected rats not treated with 4-OHT (Figs. 4A and 4B). The numbers of AADC-immunoreactive cells,

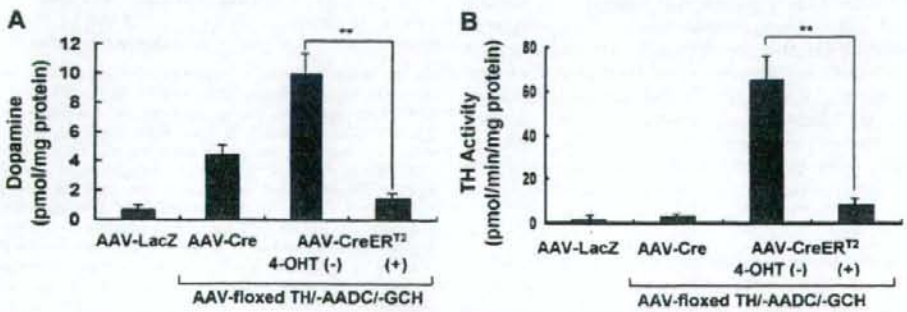

FIG. 5. Reduction of dopamine synthesis in 4-OHT-treated rats. Significantly less (A) dopamine content and (B) TH activity were observed in the lesioned striatum of 4-OHT-treated rats 12 weeks after vector injection, compared to 4-OHT-untreated rats. $^{**}P < 0.01$, $n = 4$.

doi:10.1016/j.ymthe.2005.08.009

however, did not differ significantly between 4-OHT-treated and untreated rats. We roughly estimated the number of transduced cells in the striatum at 5×10^4 based on cell counts performed on the tissue sections. This efficiency of transduction is sufficient to parallel the functional effects on behavior observed in other studies [3,5,11]. Double-labeling with both anti-Cre and anti-TH antibodies, or with anti-Cre and anti-AADC antibodies, showed that more than 80% of Cre-immunoreactive cells were also positive for TH (164 of 200) and AADC (176 of 200) in three 4-OHT-untreated rats (Fig. 4C). Immunostaining for glial fibrillary acidic protein (GFAP) or AADC in parallel sections demonstrated transduction of striatal cells without obvious reactive astrocytosis (Fig. 4D). Dopamine content (Fig. 5A) and TH activity (Fig. 5B) within the lesioned striatum were significantly lower in 4-OHT-treated compared to untreated rats. Dopamine levels in the transduced striatum in the 4-OHT-treated and untreated rats were 0.66 and 4.3%, respectively, those of the unlesioned striatum. Unlike primary dopamine in the nigrostriatal system, which is stored in synaptic vesicles, genetically produced dopamine in the lesioned striatum might be readily metabolized without storage. Since the dopamine level in the lesioned side of AAV-LacZ-injected rats was much lower (0.3%), a 10-fold increase in dopamine level after triple transduction with TH, AADC, and GCH genes caused a remarkable therapeutic effect. Average TH activity, measured in terms of L-dopa production (pmol/min/mg protein), reached 51.6% that of the normal striatum (65.9 ± 11.0 versus 127.7 ± 3.7) in rats transduced with dopamine-synthesizing enzymes. In 4-OHT-treated rats, TH activity fell to 10.8% of normal (13.8 ± 4.1).

Discussion

Our results show efficient viral vector-mediated delivery of tamoxifen-dependent CreER^{T2} recombinase into rodent brains and that transgenic floxed sequences can be deleted in a temporally controlled manner. In a rat model of PD, recombinant AAV vector-mediated delivery of CreER^{T2} into the striatum enabled 4-OHT-induced excision of a floxed TH transgene, resulting in reduced virally mediated dopamine synthesis. We targeted TH, a rate-limiting enzyme for dopamine biosynthesis that converts dietary L-tyrosine to L-dopa. Using this strategy, AADC activity was retained so that L-dopa, a substrate for AADC capable of crossing the blood–brain barrier, could be converted to dopamine in the striatum. Thus, in clinical situations, the therapeutic effects of orally administered L-dopa would likely be preserved, even after 4-OHT treatment to reduce TH expression in cases of dopamine overproduction [11]. Although transduction with AADC alone, in combination with oral administration of L-dopa, might not achieve continuous delivery of L-dopa, in contrast to that which could potentially be achieved with triple transduction of TH, AADC, and GCH, dopamine production could be regulated by altering the dose of L-dopa, thereby providing a safer option for gene therapy. We previously demonstrated that dopamine synthesis was enhanced (greater than fivefold) after systemic administration of L-dopa in AAV-TH/-AADC/-GCH-injected striatum in the primate model of PD using *in vivo* dialysis [4]. A phase I clinical trial involving gene transfer of AADC alone is currently under way.

AAV vectors are powerful tools by which to deliver therapeutic genes into the mammalian brain. Many striatal neurons of rodents and nonhuman primates are transduced with AAV vectors via stereotaxic injection, and long-term gene expression has been achieved without substantial toxicity or immune response [2,12]. AAV vectors have safety advantages over other viral vectors when it comes to *in vivo* gene delivery, since they are derived from nonpathogenic wild-type viruses. Moreover, most recombinant AAVs are present in cells as episomes, thus reducing the probability of insertional activation of oncogenes, compared to retroviruses, which integrate into host chromosomes [13]. Although it is difficult to use a single AAV vector for multiple gene transfer due to its limited packaging capacity (< 5 kb), a single cell can be simultaneously transduced with multiple AAV vectors. In the present study, dual immunofluorescence staining showed efficient cotransduction of cells with different AAV vectors in the rat striatum, a finding consistent with that which we observed in a previous study [5].

Gene therapy strategies for the treatment of PD using AAV vectors include gene delivery of dopamine-synthesizing enzymes into the striatum to restore dopamine production, as well as gene delivery of neuroprotective molecules, such as glial cell line-derived neurotrophic factor, to block or slow down further degeneration [14]. In addition, AAV vectors harboring genes encoding neurotrophic factors might be delivered by intramuscular administration in an attempt to protect spinal motoneurons in patients suffering from amyotrophic lateral sclerosis [15–17]. Although no adverse effects due to overexpression of transgenes have been reported in animals to date, it is necessary to develop vectors that allow for regulation of transgene expression, thus avoiding transgene overexpression. In PD, overproduction of dopamine has the potential to cause dyskinesia or hallucinations, and sustained exposure to high concentrations of neurotrophic factors could result in tumor formation.

Inducible Cre recombinases have been used to generate a number of conditional knockout mice. They are invaluable tools for investigators studying the role of gene function in development, as well as a number of physiological and pathological processes. The tamoxifen-dependent CreER^{T2} recombinase has proven particularly helpful [9,18,19]. It has been shown that 4-OHT does not alter dopamine content within the striatum in mice [20],

and we did not observe any adverse effects of 4-OHT treatment in the present experiment. In addition, tamoxifen, which is metabolized by the liver into 4-OHT, has neuroprotective effects [21,22]. Thus, the CreER^{T2} system might be useful for gene therapy in the treatment of neurological diseases.

We have expanded upon the use of inducible Cre recombinase technology to regulate transgene expression using an AAV vector-mediated gene delivery system. Recently, a viral vector-mediated RNA interference (RNAi) approach has been developed and localized gene knockdown achieved in the adult brain [23–25]. Although RNAi-mediated suppression of gene function has a wide variety of applications, more specific and inducible transgene silencing can be achieved with AAV-CreER^{T2}. Selective ablation of floxed transgenes reduces the possibility of down-regulation of normal cellular proteins. This system works as a molecular switch, increasing the safety of long-acting gene therapy by avoiding or minimizing side effects due to overproduction of the protein product and by providing the ability to shut down expression if toxicities are encountered or treatment is completed. The ability to restrict somatic recombination of transgenes spatially and temporally has a wide range of applications, in both gene therapy and biological study requiring somatic genetic manipulation.

Materials and Methods

AAV vector production. The AAV vector plasmids contained an expression cassette with a human cytomegalovirus immediate-early promoter (CMV promoter), followed by the first intron of human growth hormone, target cDNA, and a simian virus 40 polyadenylation signal sequence (SV40 poly(A)), between the inverted terminal repeats of the AAV-2 genome. The plasmids pAAV-LacZ, pEGFP, pAAV-AADC, pAAV-GCH, pCre, and pCreER^{T2} contained the cDNAs of LacZ, EGFP, human AADC, human GCH, Cre recombinase with a nuclear localization signal [26], and Cre recombinase fused to a mutated form of the ligand-binding domain of estrogen receptor α (CreER^{T2})[27], respectively. The plasmid pAAV-floxed TH contained human TH1 cDNA flanked by two loxP sequences between the CMV promoter and the SV40 poly(A). To generate pAAV-EGFP/Red, a DNA fragment containing d2EGFP (BD Biosciences, San Jose, CA, USA) and the SV40 poly(A) was flanked by loxP sequences and inserted between the CMV promoter and DsRed-Express-DR (BD Biosciences). The two helper plasmids, pHLP19 and pladeno1 (Avigen, Alameda, CA, USA), harbored the AAV *rep* and *cap* genes, as well as the *E2A*, *E4*, and *VA RNA* genes of the adenovirus genome, respectively. HEK293 cells were cotransfected by the calcium phosphate coprecipitation method with the vector plasmid, pHLP19, and pladeno1. The AAV vectors were then harvested and purified by two rounds of continuous iodoxale ultracentrifugations. Vector titers were determined by quantitative DNA dot-blot hybridization or by quantitative PCR of DNase I-treated vector stocks. We routinely obtained 10^{12} to 10^{13} vector genome copies (vg).

In vitro transduction. HEK293 cells were seeded at 3×10^5 cells/well in six-well plates. After 24 h, cells were infected with appropriate combinations of AAV vectors (5×10^9 vg per vector). 4-OHT was added to the culture medium at a concentration of 10 or 100 nM at 5 h after infection. Culture medium was collected for dopamine assay 48 h after infection and the cells were fixed for immunostaining.

AAV injections. All animal experiments were performed in accordance with the institutional guidelines. Three B6,129-*Gt(ROSA))26Sor*^{tm25lw}/J mice (The Jackson Laboratory, Bar Harbor, ME, USA) [10] were stereotaxically injected into the caudoputaminal unit or cerebral cortex with 1×10^9 vg (1 μl) of AAV-CreER^{T2}. After 1 week, 4-OHT (1 mg) was administered intraperitoneally every day for 5 days, after which 2 of the mice were killed. One mouse that did not receive 4-OHT treatment was killed as a control. Creation of PD model rats and stereotaxic injections of AAV vectors were carried out as previously described [5]. Briefly, 60 male albino Wistar rats (weighing 200–250 g) were unilaterally lesioned at the left medial forebrain bundle (coordinates AP − 4.3 mm and ML 1.6 mm, relative to the bregma, and DV − 7.8 mm relative to the dura, with the incisor bar set 3.3 mm below the interaural line) with 4 μl of 4.5 mg/ml 6-OHDA HBr (Sigma, St. Louis, MO, USA) in 0.02% ascorbate saline prior to intrastriatal transduction. These rats were stereotaxically injected with AAV vectors (5×10^7 vg per site for each vector) at three sites in the lesioned striatum (coordinates relative to the bregma and dura, AP +1.5, +1.0, and +0.5 mm; ML 2.6, 3.0, and 3.2 mm; DV − 5.2 mm). Forty-eight rats were injected with a 1:1:1 mixture of AAV-floxed TH, AAV-AADC, and AAV-GCH plus AAV-Cre (n = 12) or AAV-CreER^{T2} (n = 36). Twelve rats received AAV-LacZ alone as a control. Among the AAV-CreER^{T2}-treated rats, 24 were intraperitoneally injected with 4-OHT (4 mg/kg) for 5 consecutive days, starting either at the same time as or 4 weeks after vector injection.

Behavioral testing. The rats were tested weekly for rotational behavior and spontaneous limb use, as described previously [28]. The total number of complete body turns was counted during an observation period of ≥60 min following intraperitoneal injection of apomorphine HCl (0.1 mg/kg; Sigma). Only those animals exhibiting seven or more contralateral rotations/min in a 60-min period at 4 weeks after the 6-OHDA injection were included in further analysis. Spontaneous limb use was scored according to the cylinder test method [29]. Rats were placed in a clear glass cylinder large enough to ensure free movement. After they had performed 10 rears during which they were observed to place at least one paw on the cylinder wall, the number of times both forepaws contacted the wall of the cylinder was counted until at least 20 contacts were made. Data indicating the number of times a contralateral forepaw made contact with the wall are expressed as a percentage of the total. We also evaluated rotational behavior in response to a low dose of L-dopa methyl ester (5 mg/kg; Sigma) coadministered with 2.5 mg/kg of a peripheral decarboxylase inhibitor (benserazide hydrochloride; Sigma) 10 weeks after AAV injection.

Biochemical assays. Levels of dopamine in the cell culture medium (n=4 for each group) and within the brain samples (n=4 for each group) were determined by high-performance liquid chromatography (HPLC), as previously described [5]. Rats were killed by decapitation under sodium pentobarbital anesthesia 12 weeks after vector injection, after which their brains were immediately dissected and placed on dry ice. The striatum was punched out bilaterally using a sharp-edged, stainless steel tube. Wet tissue samples were weighed and stored at −80°C until subsequent analysis. Tissues were homogenized in 20 volumes of homogenization buffer and then mixed immediately with 0.76 M perchloric acid prior to centrifugation at 15,000g for 10 min. After the supernatant was neutralized with sodium acetate, the samples were analyzed by HPLC analysis. Determination of TH activity was based on the formation of L-dopa from L-tyrosine, as demonstrated by HPLC electrochemical detection. The reaction mixture contained 200 mM sodium acetate buffer (pH 6.0), 100 mM 2-mercaptoethanol, 0.2 mg/ml catalase, 0.2 mM L-tyrosine, and 1 mM tetrahydrobiopterin. The mixture was incubated for 10 min at 37°C. The reaction was stopped by adding perchloric acid, and L-dopa was extracted using an alumina column [30].

Immunostaining of cultured cells and brain sections. Cultured cells were fixed in 4% paraformaldehyde (PFA) in PBS. Brains were perfused with 4% PFA, soaked in 30% sucrose, and dissected into coronal sections (30 μm). The following primary antibodies were used: TH monoclonal (1:800 or 1:8000; DiaSorin, Stillwater, MN, USA) or polyclonal (1:10,000; provided by Ikuko Nagatsu, Fujita Health University, Japan), AADC polyclonal (1:10,000; I. Nagatsu), Cre recombinase monoclonal (1:500; Covance, Princeton, NJ, USA) or polyclonal (1:500; Covance), GFP polyclonal (1:200; BD Biosciences or Chemicon, Temecula, CA, USA), DsRed

doi:10.1016/j.ymthe.2005.08.009

polyclonal (1:1000; BD Biosciences), and GFAP (1:1000; Chemicon). Appropriate fluorescence-tagged (Invitrogen, Carlsbad, CA, USA) or biotinylated (Vector Laboratories, Burlingame, CA, USA) secondary antibodies were used for visualization. Immunoreactivity was assessed under microscopy (Axioplan, Zeiss, Germany) or confocal laser scanning microscopy (TCS NT; Leica Microsystems, Germany). To analyze quantitatively the numbers of TH-positive neurons and AADC-positive neurons, every 10th 30-μm section (total of 11 sections) covering a 3-mm thickness from each animal ($n = 3$ per group) was examined. Coexpression efficacy was analyzed by dual immunofluorescence staining.

Statistical analysis. One-way analysis of variance (ANOVA) was performed to determine differences in dopamine levels, as well as TH activity, followed by Tukey's test (StatView 5.0 software; Abacus). Behavioral changes were analyzed by a repeated measure ANOVA, followed by Tukey's test, with $P < 0.05$ considered statistically significant. Results are presented as means ± SEM.

ACKNOWLEDGMENTS

We thank Avigen, Inc., for providing the AAV vector production system. This work was supported by grants from the Ministry of Education, Science, Sports, and Culture, as well as by funds made available by the Japanese Government for a High-Tech Research Center Project for Private Universities (2003–2005) and a University–Industry Joint Research Project (2003–2005). In addition, we received grants from the Japan Ministry of Health, Labor, and Welfare; a grant from The Ministere de l'Education Nationale, de l'Enseignement Superieur et de la Recherche; and funds from The Cell Science Research Foundation, the Centre National de la Recherche Scientifique, the Institut National de la Santé et de la Recherche Médicale, and the Collège de France.

RECEIVED FOR PUBLICATION MAY 14, 2005; REVISED JULY 26, 2005; ACCEPTED AUGUST 1, 2005.

REFERENCES

1. Burton, E. A., Glorioso, J. C., and Fink, D. J. (2003). Gene therapy progress and prospects: Parkinson's disease. *Gene Ther.* **10:** 1721–1727.
2. Muramatsu, S., *et al.* (2003). Adeno-associated viral vectors for Parkinson's disease. *Int. Rev. Neurobiol.* **55:** 205–222.
3. Mandel, R. J., *et al.* (1998). Characterization of intrastriatal recombinant adeno-associated virus-mediated gene transfer of human tyrosine hydroxylase and human GTP-cyclohydrolase I in a rat model of Parkinson's disease. *J. Neurosci.* **18:** 4271–4284.
4. Muramatsu, S., *et al.* (2002). Behavioral recovery in a primate model of Parkinson's disease by triple transduction of striatal cells with adeno-associated viral vectors expressing dopamine-synthesizing enzymes. *Hum. Gene Ther.* **13:** 345–354.
5. Shen, Y., *et al.* (2000). Triple transduction with adeno-associated virus vectors expressing tyrosine hydroxylase, aromatic-L-amino-acid decarboxylase, and GTP cyclohydrolase I for gene therapy of Parkinson's disease. *Hum. Gene Ther.* **11:** 1509–1519.
6. Rajewsky, K., *et al.* (1996). Conditional gene targeting. *J. Clin. Invest.* **98:** 600–603.
7. Branda, C. S., and Dymecki, S. M. (2004). Talking about a revolution: the impact of site-specific recombinases on genetic analyses in mice. *Dev. Cell* **6:** 7–28.
8. Metzger, D., and Feil, R. (1999). Engineering the mouse genome by site-specific recombination. *Curr. Opin. Biotechnol.* **10:** 470–476.
9. Metzger, D., *et al.* (2003). Targeted conditional somatic mutagenesis in the mouse: temporally-controlled knock out of retinoid receptors in epidermal keratinocytes. *Methods Enzymol.* **364:** 379–408.
10. Mao, X., *et al.* (2001). Activation of EGFP expression by Cre-mediated excision in a new ROSA26 reporter mouse strain. *Blood* **97:** 324–326.
11. Sanchez-Pernaute, R., Harvey-White, J., Cunningham, J., and Bankiewicz, K. S. (2001). Functional effect of adeno-associated virus mediated gene transfer of aromatic L-amino acid decarboxylase into the striatum of 6-OHDA-lesioned rats. *Mol. Ther.* **4:** 324–330.
12. Tenenbaum, L., *et al.* (2004). Recombinant AAV-mediated gene delivery to the central nervous system. *J. Gene Med.* **6**(Suppl. 1): S212–S222.
13. McCarty, D. M., Young, S. M., Jr., and Samulski, R. J. (2004). Integration of adeno-associated virus (AAV) and recombinant AAV vectors. *Annu. Rev. Genet.* **38:** 819–845.
14. Hurelbrink, C. B., and Barker, R. A. (2004). The potential of GDNF as a treatment for Parkinson's disease. *Exp. Neurol.* **185:** 1–6.
15. Azzouz, M., *et al.* (2004). VEGF delivery with retrogradely transported lentivector prolongs survival in a mouse ALS model. *Nature* **429:** 413–417.
16. Kaspar, B. K., *et al.* (2003). Retrograde viral delivery of IGF-1 prolongs survival in a mouse ALS model. *Science* **301:** 839–842.
17. Wang, L. J., *et al.* (2002). Neuroprotective effects of glial cell line-derived neurotrophic factor mediated by an adeno-associated virus vector in a transgenic animal model of amyotrophic lateral sclerosis. *J. Neurosci.* **22:** 6920–6928.
18. Imai, T., *et al.* (2004). Peroxisome proliferator-activated receptor gamma is required in mature white and brown adipocytes for their survival in the mouse. *Proc. Natl. Acad. Sci. USA* **101:** 4543–4547.
19. Simon, D., *et al.* (2004). Friedreich ataxia mouse models with progressive cerebellar and sensory ataxia reveal autophagic neurodegeneration in dorsal root ganglia. *J. Neurosci.* **24:** 1987–1995.
20. Kuo, Y. M., *et al.* (2003). 4-Hydroxytamoxifen attenuates methamphetamine-induced nigrostriatal dopaminergic toxicity in intact and gonadectomized mice. *J. Neurochem.* **87:** 1436–1443.
21. Ciriza, I., *et al.* (2004). Selective estrogen receptor modulators protect hippocampal neurons from kainic acid excitotoxicity: differences with the effect of estradiol. *J. Neurobiol.* **61:** 209–221.
22. Obata, T., and Kubota, S. (2001). Protective effect of tamoxifen on 1-methyl-4-phenylpyridine-induced hydroxyl radical generation in the rat striatum. *Neurosci. Lett.* **308:** 87–90.
23. Harper, S. Q., *et al.* (2005). RNA interference improves motor and neuropathological abnormalities in a Huntington's disease mouse model. *Proc. Natl. Acad. Sci. USA* **102:** 5820–5825.
24. Hommel, J. D., *et al.* (2003). Local gene knockdown in the brain using viral-mediated RNA interference. *Nat. Med.* **9:** 1539–1544.
25. Xia, H., *et al.* (2004). RNAi suppresses polyglutamine-induced neurodegeneration in a model of spinocerebellar ataxia. *Nat. Med.* **10:** 816–820.
26. Kalderon, D., Roberts, B. L., Richardson, W. D., and Smith, A. E. (1984). A short amino acid sequence able to specify nuclear location. *Cell* **39:** 499–509.
27. Feil, R., Wagner, J., Metzger, D., and Chambon, P. (1997). Regulation of Cre recombinase activity by mutated estrogen receptor ligand-binding domains. *Biochem. Biophys. Res. Commun.* **237:** 752–757.
28. Wang, L., *et al.* (2002). Delayed delivery of AAV-GDNF prevents nigral neurodegeneration and promotes functional recovery in a rat model of Parkinson's disease. *Gene Ther.* **9:** 381–389.
29. Schallert, T., *et al.* (2000). CNS plasticity and assessment of forelimb sensorimotor outcome in unilateral rat models of stroke, cortical ablation, parkinsonism and spinal cord injury. *Neuropharmacology* **39:** 777–787.
30. Nagatsu, T., Oka, K., and Kato, T. (1979). Highly sensitive assay for tyrosine hydroxylase activity by high-performance liquid chromatography. *J. Chromatogr.* **163:** 247–252.

STEM CELLS®

Improved Safety of Hematopoietic Transplantation with Monkey Embryonic Stem Cells in the Allogeneic Setting

Hiroaki Shibata, Naohide Ageyama, Yujiro Tanaka, Yukiko Kishi, Kyoko Sasaki, Shinichiro Nakamura, Shin-ichi Muramatsu, Satoshi Hayashi, Yoshihiro Kitano, Keiji Terao and Yutaka Hanazono

Stem Cells 2006;24;1450-1457; originally published online Feb 2, 2006;
DOI: 10.1634/stemcells.2005-0391

STEM CELLS
EMBRYONIC STEM CELLS

Improved Safety of Hematopoietic Transplantation with Monkey Embryonic Stem Cells in the Allogeneic Setting

HIROAKI SHIBATA,[a,b] NAOHIDE AGEYAMA,[b] YUJIRO TANAKA,[a] YUKIKO KISHI,[a] KYOKO SASAKI,[a] SHINICHIRO NAKAMURA,[b,c] SHIN-ICHI MURAMATSU,[d] SATOSHI HAYASHI,[e] YOSHIHIRO KITANO,[f] KEIJI TERAO,[b] YUTAKA HANAZONO[a]

[a]Division of Regenerative Medicine, Center for Molecular Medicine, Jichi Medical University, Tochigi, Japan; [b]Tsukuba Primate Research Center, National Institute of Biomedical Innovation, Ibaraki, Japan; [c]Department of Veterinary Pathology, Nippon Veterinary and Animal Science University, Tokyo, Japan; [d]Department of Neurology, Jichi Medical University, Tochigi, Japan; Departments of [e]Obstetrics and Gynecology and [f]Surgery, National Center for Child Hearth and Development, Tokyo, Japan

Key Words. Cynomolgus monkey • Hematopoiesis • Embryonic stem cell • In utero transplantation • Teratoma • Purging Tumor prevention

ABSTRACT

Cynomolgus monkey embryonic stem cell (cyESC)-derived in vivo hematopoiesis was examined in an allogeneic transplantation model. cyESCs were induced to differentiate into the putative hematopoietic precursors in vitro, and the cells were transplanted into the fetal cynomolgus liver at approximately the end of the first trimester (n = 3). Although cyESC-derived hematopoietic colony-forming cells were detected in the newborns (4.1%–4.7%), a teratoma developed in all newborns. The risk of tumor formation was high in this allogeneic transplantation model, given that tumors were hardly observed in immunodeficient mice or fetal sheep that had been xeno-transplanted with the same cyESC derivatives. It turned out that the cyESC-derived donor cells included a residual undifferentiated fraction positive for stage-specific embryonic antigen (SSEA)-4 (38.2% ± 10.3%) despite the rigorous differentiation culture. When an SSEA-4-negative fraction was transplanted (n = 6), the teratoma was no longer observed, whereas the cyESC-derived hematopoietic engraftment was unperturbed (2.3%–5.0%). SSEA-4 is therefore a clinically relevant pluripotency marker of primate embryonic stem cells (ESCs). Purging pluripotent cells with this surface marker would be a promising method of producing clinical progenitor cell preparations using human ESCs. STEM CELLS *2006;24:1450–1457*

INTRODUCTION

Human embryonic stem cells (hESCs) hold great potential in the treatment of a variety of diseases and injuries because embryonic stem cells (ESCs) have the ability to proliferate indefinitely in culture and to differentiate into any cell type [1, 2]. Because ESCs are able to form teratomas when transplanted into immunodeficient mice, safety concerns would be raised against the clinical application of hESCs [3, 4]. It will be necessary to test the safety of these cells in animal transplantation models before clinical application. Nonhuman primate transplantation models would be desirable for this purpose; however, there have been only a few reports on these models [5–7]. The successful engraftment of transplanted cells in primates will not be achieved unless the immune rejection of transplanted cells is circumvented (e.g., through immunosuppressive treatment) [6]. The early gestational fetus may be a good recipient with which to circumvent immune rejection because the immune system is premature [8]. In addition, in the animal fetus, transplanted cells would engraft without conditioning of recipients such as irradiation or immunosuppressive treatment [9–12]. We have previously established a system for allogeneic transplantation of cynomolgus ESCs (cyESCs) using preimmune fetal monkeys as recipients [5].

We have also reported a novel method for hematopoietic engraftment from cyESCs in sheep [13]. The method is a combination of three steps: (a) differentiation in vitro to generate the putative hematopoietic precursors [14]; (b) transplantation of the cells in utero [15]; and (c) development into hematopoietic cells in vivo using the hematopoietic microenvironment of the fetal liver [16]. In the present study,

Correspondence: Yutaka Hanazono, M.D., Ph.D., Division of Regenerative Medicine, Center for Molecular Medicine, Jichi Medical University, 3311-1 Yakushiji, Shimotsuke, Tochigi 329-0498, Japan. Telephone: +81-285-58-7450; Fax: +81-285-44-5205; e-mail: hanazono@jichi.ac.jp Received on August 13, 2005; accepted for publication on January 23, 2006; first published online in STEM CELLS *EXPRESS* February 2, 2006. 1066-5099/2006/$20.00/0 doi: 10.1634/stemcells.2005-0391

we have examined the safety as well as the efficacy of hematopoietic engraftment of cells derived from cyESCs in the allogeneic transplantation model.

MATERIALS AND METHODS

Animals

Pregnant cynomolgus monkeys (16–22 years old) were obtained by mating and were reared at the Tsukuba Primate Research Center in accordance with Rules for Animals Care and Management set forth by the Research Center and Guiding Principles for Animal Experiments Using Nonhuman Primates formulated by the Primate Society of Japan. Experimental procedures were approved by the Animal Welfare and Animal Care Committee of the National Institute of Infectious Diseases. The animals were free of intestinal parasites and were seronegative for herpes virus B, varicella-zoster-like virus, measles virus, and simian immunodeficiency virus.

Cell Preparation

A cyESC line (CMK6G) stably expressing green fluorescent protein (GFP) was established after transfection of the parental cyESC line (CMK6) with the enhanced GFP gene (Clontech, Palo Alto, CA, http://www.clontech.com) [17]. cyESCs were maintained on a feeder layer of mitomycin C (Kyowa, Tokyo, http://www.kyowa.co.jp)-treated mouse (ICR or BALB/c; Clea Japan, Tokyo, http://www.clea-japan.com) embryonic fibroblasts as previously described [18]. The mouse bone marrow stromal cell line OP9 was maintained in α-minimum essential medium (Invitrogen, Carlsbad, CA, http://www.invitrogen.com) supplemented with 20% fetal calf serum (FCS; Invitrogen) [19].

cyESCs were induced to differentiate into the putative hematopoietic precursors as previously described [13]. Briefly, undifferentiated cyESCs were transferred onto mitomycin C-treated confluent OP9 cells and cultured for 6 days in Iscove's modified Dulbecco's medium (Invitrogen) supplemented with 8% FCS, 8% horse serum (Invitrogen), 5×10^{-6} M hydrocortisone (Sigma, St. Louis, http://www.sigmaaldrich.com), and multiple cytokines, including 20 ng/ml recombinant human (rh) bone morphogenetic protein-4 (R&D Systems, Minneapolis, http://www.rndsystems.com), 20 ng/ml rh stem cell factor (Biosource, Camarillo, CA, http://www.biosource.com), 20 ng/ml rh vascular endothelial growth factor (VEGF; R&D Systems), 20 ng/ml rh Flt-3 ligand (PeproTech, Rocky Hill, NJ, http://www.peprotech.com), 20 ng/ml rh interleukin-3 (PeproTech), 10 ng/ml rh interleukin-6 (PeproTech), 20 ng/ml rh granulocyte colony-stimulating factor (PeproTech), and 2 IU/ml rh erythropoietin (Roche, Basel, Switzerland, http://www.roche.com). The cells were resuspended in 0.1% human serum albumin (Sigma)/Hanks' balanced saline solution (Sigma) for transplantation.

Flow Cytometry

Primary antibodies (Abs) used in the present study were anti-human CD34 monoclonal Ab (mAb; BD Pharmingen, San Diego, http://www.bdbiosciences.com/pharmingen), anti-human CD31 mAb (Pharmingen), anti-human CD45 mAb (Pharmingen), anti-human vascular endothelial (VE) cadherin mAb (Pharmingen), rabbit anti-human VEGF receptor (VEGFR)-2 Ab (Santa Cruz Biotechnology, Santa Cruz, CA, http://www.scbt.com), and anti-stage-specific embryonic antigen (SSEA)-4 mAb (Chemicon, Temecula, CA, http://www.chemicon.com). All of them cross-reacted to cynomolgus counterparts as previously demonstrated [18, 20–22]. Secondary Abs were phycoerythrin (PE)-conjugated rabbit anti-mouse immunoglobulins (Ig) Ab (DakoCytomation, Glostrup, Denmark, http://www.dako.com) and Alexa Fluor 647-conjugated goat anti-mouse IgG Ab (Molecular Probes, Eugene, OR, http://probes.invitrogen.com). Cells stained with unlabeled primary Abs were incubated with fluorescence-labeled secondary Abs. Cells were incubated with either primary or secondary Ab for 20–60 minutes at 4°C. Regarding staining with the anti-VEGFR-2 Ab, the cells were incubated with biotin-conjugated goat anti-rabbit IgG Ab (Beckman Coulter, Miami, http://www.beckmancoulter.com), followed by PE-conjugated streptavidin (Beckman Coulter). Fluorescence-labeled cells were analyzed with a FACS Calibur flow cytometer (Becton, Dickinson and Company, Franklin Lakes, NJ, http://www.bd.com). Data analysis was performed using the CellQuest software (Becton, Dickinson and Company). Isotype-matched, irrelevant mAbs (DakoCytomation or Beckman Coulter) served as negative controls. Nonviable cells were excluded from analysis by propidium iodide (Sigma) costaining.

Cell Sorting

Cell sorting was performed to purge SSEA-4$^+$ cells from among the cultured cyESCs in vitro. Cells were incubated with the anti-SSEA-4 mAb for 1 hour at 4°C and washed twice with Dulbecco's modified Eagle's medium supplemented with 10% FCS. The cells were then incubated with the PE-conjugated anti-mouse Ig Ab for 1 hour at 4°C and washed twice again. GFP-positive and SSEA-4-negative cells were sorted using an Epics Elite cell sorter (Beckman Coulter). Data acquisition was performed using the Expo2 software (Beckman Coulter).

Transplantation and Delivery

Transplant procedures were previously described [5]. Briefly, animals were anesthetized via an intramuscular administration of ketamine hydrochloride (Ketalar, 10 mg/kg; Sankyo, Tokyo, http://www.sankyo.co.jp) and received 0.5%–1.0% isoflurane by inhalation by means of an endotracheal tube. Cells ($0.16–46 \times 10^6$ cells per fetus; Table 1) were injected into the fetal liver through a 23-gauge needle using an ultrasound-guided technique at approximately the end of the first trimester. The fetuses were delivered by cesarean section at 2–3 months after transplant (gestation 120–157 days, full term 165 days).

Colony Polymerase Chain Reaction

Cynomolgus clonogenic hematopoietic colonies were produced as previously described [20]. After cells were cultured in methylcellulose medium for 10–14 days, well-separated individual colonies were plucked into 50 μl of distilled water and digested with 20 μg/ml proteinase K (Takara, Shiga, Japan, http://www.takara-bio.com) at 55°C for 1 hour, followed by 99°C for 10 minutes. Each sample (5 μl) was used for a nested polymerase chain reaction (PCR) to detect the *GFP* gene sequence. The outer primer set was 5′-AAGGACGACGGCAACTACAA-3′ and 5′-ACTGGGTGCTCAGGTAGTGG-3′, and the inner primer set was 5′-GCATCGACTTCAAGGAGGAC-3′ and 5′-GTTGTGGCGGATCTTGAAGT-3′. Amplification conditions for both the outer and inner PCR were 30 cycles of 95°C for 30 seconds, 65°C for 30 seconds, and 72°C for 30 seconds. The

Table 1. ESC-derived hematopoiesis and tumor formation

Animals	Animal no.	Transplanted cells	Purging SSEA-4$^+$ cells	Cell number per fetus ($\times 10^6$)	Donor-derived CFU in recipients[a] at birth (donor/total colony number)	Tumor formation	Observation period (months)
Monkeys	0031	Undifferentiated	−	3.90	n.d.	+	3
	2311	ESCs	−	0.16	n.d., Dead	+	2
	0321		−	0.21	n.d., Dead	+	2
	0841	Day-6 ESC-	−	10	4.1% (2/49)	+	3
	1551	derived cells	−	46	n.d., Dead	+	2.5
	0021		−	46	4.7% (4/85)	+	3
	0691	Day-6 ESC-	+	0.16	3.2% (2/62)	−	3
	0381	derived cells	+	1.40	5.0% (4/80)	−	3
	0022		+	0.17	2.3% (2/86)	−	3
	0981		+	0.31	4.1% (3/73)	−	3
	0051		+	0.31	n.d., Dead[b]	−	3
	1552		+	0.75	4.4% (2/45)	−	4
Sheep[c]	57	Day-6 ESC-	−	50	1.1% (1/91)	−	18
	55	derived cells	−	50	1.1% (1/91)	−	26
	141		−	78	1.1% (1/91)	−	26
	182		−	14	1.6% (1/63)	−	21

[a]Percentage of donor-derived CFU was calculated by dividing the number of CFU positive for the green fluorescent protein gene sequence by the number of CFU positive for the β-actin gene sequence. Donor-derived CFU were analyzed at delivery.
[b]Death due to ablation of placentae. Other deaths were presumably tumor-related.
[c]As published by Sasaki et al. [13].
Abbreviations: CFU, colony-forming units; ESC, embryonic stem cell; n.d., not done; SSEA, stage-specific embryonic antigen.

outer PCR products were purified using a QIA quick PCR purification kit (Qiagen, Valencia, CA, http://www.qiagen.com). Simultaneous PCR for the β-actin sequence was also performed to ensure DNA amplification of the sample in each colony. The primer set for β-actin was 5′-CATTGTCATGGACTCTGGCGACGG-3′ and 5′-CATCTCCTGCTCGAAGTCTAGGGC-3′. Amplification conditions for β-actin PCR were 40 cycles of 95°C for 30 seconds, 65°C for 30 seconds, and 72°C for 30 seconds. Amplified GFP (131 bp) and β-actin (234 bp) products were resolved on 2% agarose gel (Sigma) and visualized by ethidium bromide (Invitrogen) staining.

RNA PCR

Total RNA was extracted from cells of interest using the EZ1 RNA universal tissue kit (Qiagen). RNA was reverse-transcribed at 50°C for 30 minutes using the RNA LA PCR kit (Takara) with oligo dT primer. The resulting cDNA was then subjected to PCR. Regarding PCR for Oct-4, the primer set was 5′-GGACACCTGGCTTCGGATT-3′ and 5′-TTCGCTTTCTCTTTCGGGC-3′. The PCR conditions were 35 cycles of 95°C for 30 seconds, 67°C for 45 seconds, and 68°C for 1.5 minutes. Regarding PCR for Scl, the primer set was 5′-GGGCGGAAAGCTGTTTGCGATT-3′ and 5′-TCGCTGAGAGGCCTGCAGTT-3′. The PCR conditions were 35 cycles of 95°C for 30 seconds, 63°C for 1 minute, and 72°C for 1 minute. A simultaneous PCR for β-actin was also conducted on each cDNA sample as an internal control as described above. Amplified Oct-4 (697 bp), Scl (201 bp), and β-actin (234 bp) products were resolved on 2% agarose gel and visualized by ethidium bromide staining.

RESULTS

In Utero Transplantation and Delivery

cyESCs stably expressing GFP were used in this study [17]. In the setting of allogeneic transplantation, GFP was used as a genetic tag to track transplanted cell progeny. We employed the OP9 stromal cell coculture method instead of the embryoid body formation method to facilitate the hematopoietic differentiation [19, 23, 24] (Fig. 1A, 1B). According to the flow cytometric analysis, CD34, CD31 (platelet/endothelial cell adhesion molecule-1 [PECAM-1]), CD144 (VE-cadherin), and VEGFR-2 (Flk-1) were all upregulated on day 6 but decreased thereafter (Fig. 1C–1E, 1G). Among the markers examined, CD34 is a widely used surface marker of hematopoietic stem cells in both human and monkey subjects [25–27]. The others are key markers of hemangioblasts (which generate endothelial and hematopoietic lineages) in both mice and humans [14, 28]. Cells positive for both VEGFR-2 and VE-cadherin emerged on day 6 (Fig. 1H). CD45, however, was not detected until day 12 (Fig. 1F). Despite the hemangioblast marker expression on day 6, the hematopoietic *Scl* gene was upregulated at this time point as assessed by RNA PCR (Fig. 1I), implying that the hematopoietic commitment might have already occurred on day 6 [29, 30]. We therefore designated the day 6 cyESC-derived progenitor cells as putative hematopoietic precursors. The time course profiles presented here were similar to those of hESCs [14, 24]. The GFP expression was stable during the 6-day culture (Fig. 1A, 1B) and afterward (data not shown).

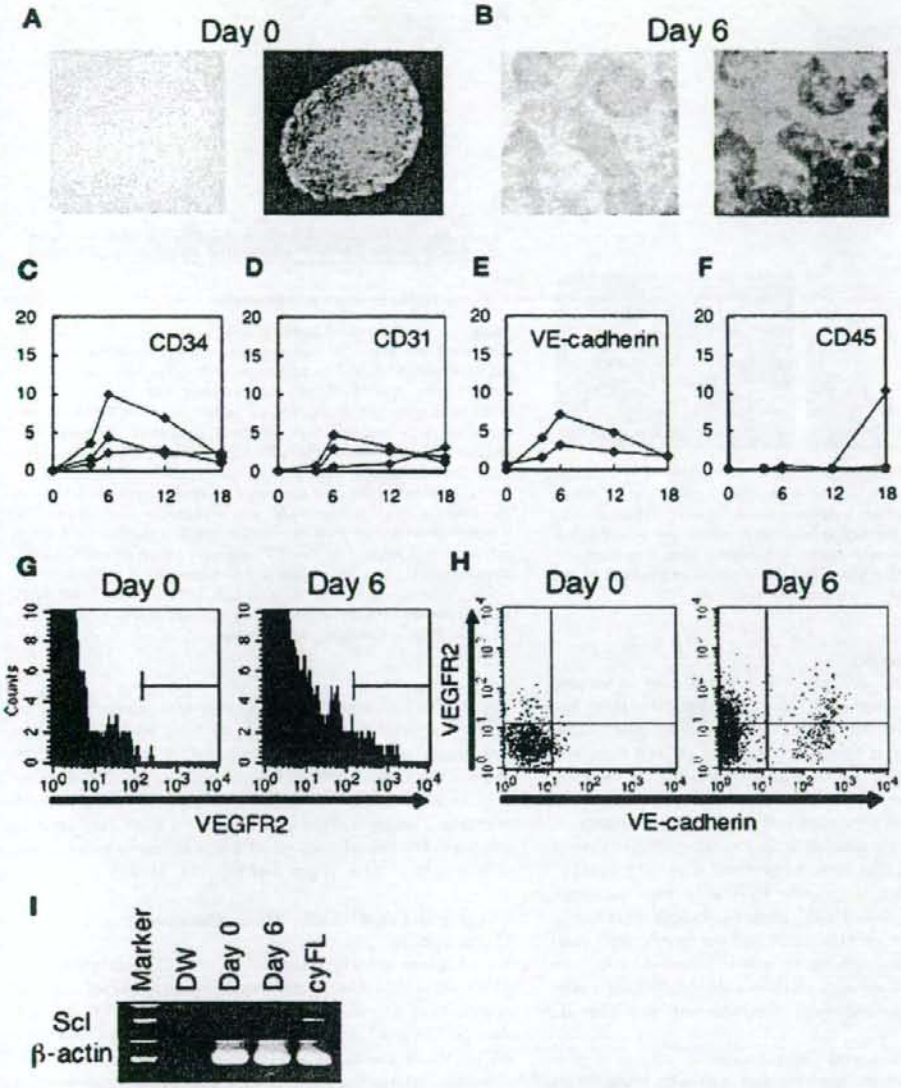

Figure 1. Flow cytometric analysis during the in vitro differentiation of cyESCs. Undifferentiated cyESCs expressing green fluorescent protein were cultured on OP9 cells with multiple cytokines (see Materials and Methods). **(A):** Cells on day 0 are shown in bright (left) and dark (right) fields. **(B):** Cells on day 6 are shown in bright (left) and dark (right) fields. **(C):** Cells on days 0, 4, 6, 12, and 18 were stained for CD34. **(D):** Cells on days 0, 4, 6, 12, and 18 were stained for CD31. **(E):** Cells on days 0, 4, 6, 12, and 18 were stained for VE-cadherin. **(F):** Cells on days 0, 4, 6, 12, and 18 were stained for CD45. The vertical axis shows the fraction (percentage) of cells that were stained positive. **(C–F):** Results of two or three independent experiments are shown. **(G):** Although cells on day 0 already express low levels of VEGFR-2, a VEGFR-2^{high} population did not emerge until day 6. **(H):** Dot-plot profiles for VEGFR-2 and VE-cadherin expression indicate that cells positive for both VEGFR-2 and VE-cadherin emerged until day 6. **(G, H):** Representative results from three independent experiments are shown. **(I):** The *Scl* gene expression was upregulated on day 6 to a level similar to that in the cynomolgus fetal liver as assessed by RNA polymerase chain reaction. Day-6 cells (putative hematopoietic precursors) were used for transplantation. Abbreviations: cyESC, cynomolgus embryonic stem cell; cyFL, cynomolgus fetal liver; DW, distilled water; VE, vascular endothelial; VEGFR, vascular endothelial growth factor receptor.

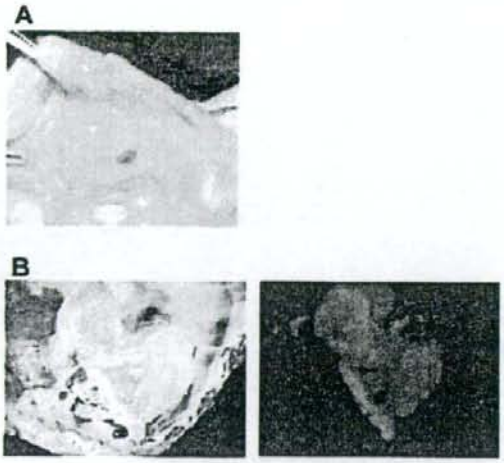

Figure 2. Tumor formation after the transplantation of cynomolgus embryonic stem cell (cyESC)-derived progenitor cells. Tumors formed in all three monkey fetuses transplanted with the day-6 cyESC-derived progenitor cells (putative hematopoietic precursors). **(A):** A representative tumor in the thoracic cavity at 3 months after transplantation (monkey no. 0841). **(B):** The tumor was observed in bright (left) and dark (right) fields under a fluorescence microscope.

Teratoma Formation

The undifferentiated cyESCs ($n = 3$) or cyESC-derived putative hematopoietic precursors ($n = 3$) were transplanted in utero into allogeneic fetuses in the liver under ultrasound guidance at approximately the end of the first trimester (49–66 days, full term 165 days) (Table 1). Regardless of whether the undifferentiated cyESCs or putative hematopoietic precursors were transplanted, tumors were found in the thoracic or abdominal cavities in all the six animals at 2–3 months after transplant (Table 1; Fig. 2A). The tumors fluoresced (Fig. 2B) and consisted of three germ layer cells. Thus, they were teratomas derived from transplanted cells. However, tumors were hardly observed in fetal sheep (1/10; [13] and our unpublished data) (Table 1) and immunodeficient (nonobese diabetic/severe combined immunodeficient) mice (3/10; our unpublished data) after the same putative hematopoietic precursors were transplanted.

In Vivo cyESC-Derived Hematopoiesis

Regarding the newborn monkeys that had been transplanted with the putative hematopoietic precursors, we harvested cells from the femur, cord blood, and liver and plated the cells in methylcellulose medium to produce clonogenic hematopoietic colonies (colony-forming units [CFU]) (Fig. 3A). The monkey cells generated colonies of clear hematopoietic morphology in this assay (Fig. 3B). To detect transplanted cell-derived, GFP-positive colonies, we tried to observe GFP fluorescence of colonies under a fluorescent microscope but were hampered by the high autofluorescence. We then conducted PCR for the *GFP* gene sequence in DNA isolated from each colony (colony PCR) (Fig. 3C). The transplanted cell-derived CFU were clearly detected in the animals (4.1% and 4.7%; Table 1). We repeated the colony PCR and confirmed that the results were reproducible.

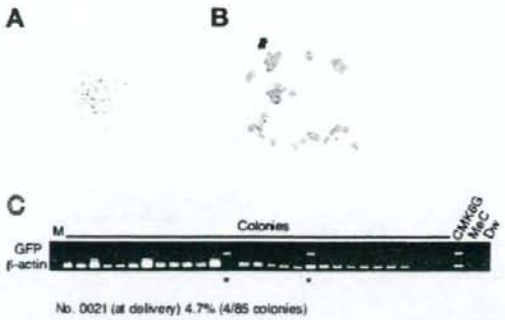

Figure 3. cyESC-derived hematopoiesis in vivo. **(A):** Bone marrow, cord blood, and liver cells were harvested from newborn monkeys and placed in methylcellulose medium to produce clonogenic hematopoietic colonies. **(B):** A cytospin specimen (stained with the May-Giemsa method) of plucked colonies reveals mature neutrophils. To identify cyESC-derived colonies, well-separated individual colonies were plucked and examined for the GFP sequence by PCR. Plucked MeC alone (not containing colonies) served as a negative control. PCR of the β-actin sequence in the same colonies was simultaneously performed as an internal control. Colony PCR was repeated at least twice. **(C):** Representative colony PCR results for monkey no. 0021. Asterisk indicates bands positive for the GFP sequence. Abbreviations: CMK6G, positive control green fluorescent protein-expressing cynomolgus cells; cyESC, cynomolgus embryonic stem cell; DW, distilled water; GFP, green fluorescent protein; M, molecular weight marker; MeC, methylcellulose; PCR, polymerase chain reaction.

We detected both granulocytic and erythroid cynomolgus CFU. In the peripheral blood, however, we were not able to detect cells expressing GFP by flow cytometry. It turned out that, as assessed by quantitative PCR, the fractions of GFP-positive cells in the peripheral blood were very small (<0.1%). Low peripheral "chimerism" has been reported more than once in other in utero transplantations of ESCs or hematopoietic stem cells such as in mice, sheep, and pigs [13, 31–33].

Purging SSEA-4$^+$ Cells of the Putative Hematopoietic Precursors

We examined the expression of an undifferentiated primate ESC marker, SSEA-4, in the undifferentiated cyESCs (day 0) and putative hematopoietic precursors (day 6). The proportion of SSEA-4$^+$ cells was 93.4% ± 8.1% and 38.2% ± 10.3% among the day-0 and -6 cells, respectively (Fig. 4A). A substantial number of cells were still positive for SSEA-4 after the rigorous differentiation culture. In addition, a considerable number of cells expressing another undifferentiated marker, Oct-4, remained among the day-6 population as assessed by RNA-PCR (Fig. 4B). Those residual undifferentiated cells might be responsible for the formation of teratomas in the recipients.

To prevent teratomas from forming in recipients, we purged SSEA-4$^+$ cells of the putative hematopoietic precursors and transplanted the SSEA-4$^-$ population into the fetal monkey liver ($n = 6$) (Fig. 4C). At delivery, tumors were no longer observed in the six animals that had been transplanted with the sorted SSEA-4$^-$ cells (Fig. 4D). The transplanted cell-derived CFU were clearly detected in the newborns, and

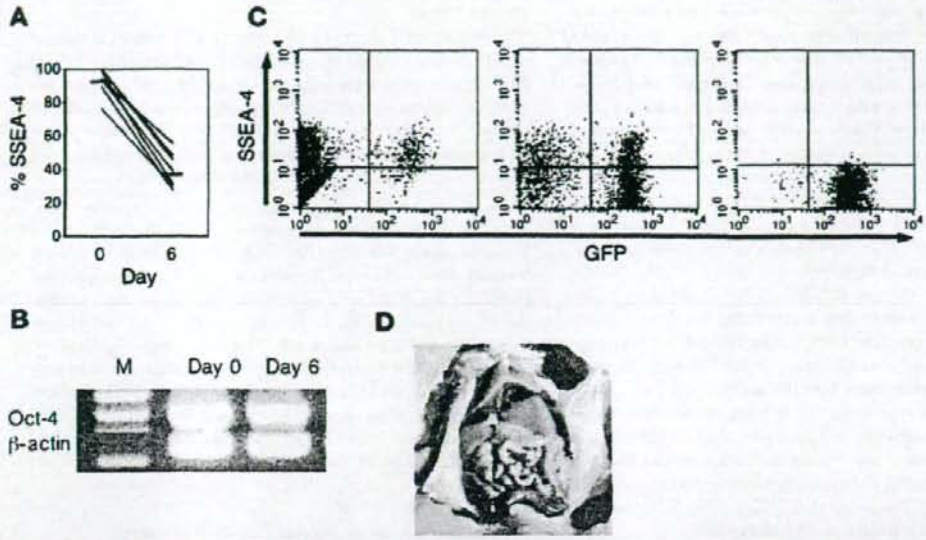

Figure 4. Purging SSEA-4$^+$ cells from among cyESC-derived progenitor cells. **(A):** Undifferentiated cyESCs (day 0) and cyESC-derivatives (day 6) were stained with anti-SSEA-4. The SSEA-4 expression (percentage of total) at day 0 and day 6 is shown ($n = 8$). **(B):** The Oct-4 expression at days 0 and 6 was also examined by RNA polymerase chain reaction. **(C):** Flow cytometric dot-plot profiles are shown for the SSEA-4 versus GFP expression at day 0 (left), at day 6 before the purge (middle), and at day 6 after the purge (right). Six independent experiments were conducted, and similar results were obtained. **(D):** No tumors were detected in any monkey after the transplantation of SSEA-4-negative day-6 cyESC derivatives (a representative monkey, no. 0981). Abbreviations: cyESC, cynomolgus embryonic stem cell; GFP, green fluorescent protein; M, molecular weight marker; SSEA, stage-specific embryonic antigen.

the fraction was not spoiled (2.3%–5.0%; Table 1), although the removed SSEA-4$^+$ fraction included some CD34$^+$ cells (data not shown).

Discussion

We have previously described a method for hematopoietic engraftment from cyESCs [13]. cyESCs were first cultured for 6 days in vitro, and the day-6 cyESC-derived putative hematopoietic precursors were transplanted in vivo into fetal sheep liver after the first trimester, generating sheep with cynomolgus hematopoiesis. We transplanted the day-6 cells because the CD34 expression level was highest at this time point (Fig. 1C). We transplanted the cells into the liver because the liver is the major hematopoietic organ at this stage of gestation in sheep [34]. In the present study, we tested this method in a cynomolgus monkey allogeneic transplantation model and successfully detected cyESC-derived hematopoietic cells in cynomolgus recipients, albeit at low levels. cyESC-derived chimerism was, however, higher in the primate allogeneic transplantation model (2.3%–5.0%) than in our recently reported sheep xeno-transplantation model (1.1%–1.6%; [13]) (Table 1). To enhance ESC-derived hematopoiesis, further consideration is required of the in vitro culture conditions (i.e., the cytokine milieu, coculture- or embryoid body-associated cellular microenvironment, culture period, and genetic manipulation) and the in utero transplantation conditions (i.e., the preconditioning, route, and timing).

Teratomas developed in all animals, even after the transplantation of ESC-derived progenitor cells that had been cultured for 6 days in the differentiation medium. The risk of tumor formation was high, given that we could hardly detect tumors in immunodeficient mice or fetal sheep that had been transplanted with the same day-6 cyESC derivatives ([13] and our unpublished data). Innate immune responses against cynomolgus-derived tumors might be more rigorous in xeno-transplanted mice and sheep than in allo-transplanted monkeys, resulting in a failure to detect tumorigenesis in the xeno-transplantation models. Similarly, Erdo et al. reported that tumors developed after ESC-derived progenitor cell transplantation in the mouse-to-mouse setting, but not in the mouse-to-rat setting [35]. Our monkey allogeneic transplantation setting would therefore allow the strict evaluation of the in vivo safety of transplantation therapies using ESCs. However, given that teratomas indeed form when undifferentiated cyESCs alone are xeno-transplanted into immunodeficient mice, it is unclear why residual undifferentiated cells included among the day-6 cyESC derivatives did not form teratomas in immunodeficient mice or fetal sheep.

SSEAs that are developmentally regulated during early embryogenesis are widely used as markers to monitor the differentiation of both mouse and human embryos and ESCs [36–38]. Undifferentiated ESCs of both human and cynomolgus origin are characterized by the expression of SSEA-4 and by a lack of SSEA-1 [1, 2, 18]. We have therefore used SSEA-4 as a marker for the negative selection of an undifferentiated fraction. As a result of this negative selection, tumors were no longer detected in the monkeys after transplantation. On the other hand, Bieberich et al. recently developed a method for selective apoptosis of residual pluripotent stem cells using the transcription

factor Oct-4 as a pluripotency marker to prevent teratoma formation [39]. They found that the expression of Oct-4 is colocalized with that of prostate apoptosis response-4, a protein mediating ceramide-induced apoptosis. Treatment of ESC-derived neural precursors with ceramide resulted in selective elimination of residual Oct-4-positive pluripotent cells. Our method, however, uses a cell surface marker to purge pluripotent cells. With this method, one can see the purging efficiency in real-time. This would be meritorious for clinical applications. Although we used a cell sorter to obtain the SSEA-4$^-$ fraction in the present study, selection with beads would be easier and more appropriate for clinical applications.

To generalize the use of SSEA-4 for eliminating undifferentiated cells from among donor cells, we differentiated cyESCs into neural stem cells. After the culture, approximately 10% of cells were still positive for SSEA-4. When all the cells were transplanted into the striatum of Parkinson's cynomolgus monkeys, teratomas developed. We then transplanted cyESC-derived neural stem cells without an SSEA-4$^+$ fraction into the cynomolgus striatum and successfully detected the engraftment without tumor formation (our unpublished data). The removal of SSEA-4$^+$ cells is useful at least for hematopoietic and neural lineages.

CONCLUSION

We are now able to prevent the formation of tumors in nonhuman primate recipients by purging SSEA-4$^+$ cells from among ESC-derived progenitor cells without spoiling the engraftment. SSEA-4 is therefore a clinically relevant pluripotency marker of primate ESCs. Purging pluripotent cells with this marker would be a promising method for producing clinical progenitor cell preparations using hESCs to improve safety in vivo.

ACKNOWLEDGMENTS

We thank Norio Nakatsuji (Kyoto University, Kyoto, Japan) and Yasushi Kondo (Tanabe Seiyaku Co., Ltd., Osaka, Japan) for providing cyESCs; Toru Nakano (Osaka University, Osaka, Japan) for providing OP9 cells; and Naomi Terao and Naomi Takino for technical assistance. This study was supported by grants (JMS 21st Century COE program, High-tech Research Center program, and Creation of Innovations) from the Ministry of Education, Culture, Sports, Science and Technology of Japan as well as grants (KAKENHI) from the Ministry of Health, Labor and Welfare of Japan.

DISCLOSURES

The authors indicate no potential conflicts of interest.

REFERENCES

1 Thomson JA, Itskovitz-Eldor J, Shapiro SS et al. Embryonic stem cell lines derived from human blastocysts. Science 1998;282:1145–1147.

2 Reubinoff BE, Pera MF, Fong CY et al. Embryonic stem cell lines from human blastocysts: Somatic differentiation in vitro. Nat Biotechnol 2000; 18:399–404.

3 Bjorklund LM, Sanchez-Pernaute R, Chung S et al. Embryonic stem cells develop into functional dopaminergic neurons after transplantation in a Parkinson rat model. Proc Natl Acad Sci U S A 2002;99: 2344–2349.

4 Fujikawa T, Oh SH, Pi L et al. Teratoma formation leads to failure of treatment for type I diabetes using embryonic stem cell-derived insulin-producing cells. Am J Pathol 2005;166:1781–1791.

5 Asano T, Ageyama N, Takeuchi K et al. Engraftment and tumor formation after allogeneic in utero transplantation of primate embryonic stem cells. Transplantation 2003;76:1061–1067.

6 Takagi Y, Takahashi J, Saiki H et al. Dopaminergic neurons generated from monkey embryonic stem cells function in a Parkinson primate model. J Clin Invest 2005;115:102–109.

7 Sanchez-Pernaute R, Studer L, Ferrari D et al. Long-term survival of dopamine neurons derived from parthenogenetic primate embryonic stem cells (Cyno-1) after transplantation. STEM CELLS 2005;23: 914–922.

8 Darrasse-Jeze G, Marodon G, Salomon BL et al. Ontogeny of CD4$^+$CD25$^+$ regulatory/suppressor T cells in human fetuses. Blood 2005;105:4715–4721.

9 Harrison MR, Slotnick RN, Crombleholme TM et al. In-utero transplantation of fetal liver haemopoietic stem cells in monkeys. Lancet 1989;2: 1425–1427.

10 Zanjani ED, Mackintosh FR, Harrison MR. Hematopoietic chimerism in sheep and nonhuman primates by in utero transplantation of fetal hematopoietic stem cells. Blood Cells 1991;17:349–366.

11 Cowan MJ, Tarantal AF, Capper J et al. Long-term engraftment following in utero T cell-depleted parental marrow transplantation into fetal rhesus monkeys. Bone Marrow Transplant 1996;17:1157–1165.

12 Tarantal AF, Goldstein O, Barley F et al. Transplantation of human peripheral blood stem cells into fetal rhesus monkeys (*Macaca mulatta*). Transplantation 2000;69:1818–1823.

13 Sasaki K, Nagao Y, Kitano Y et al. Hematopoietic microchimerism in sheep after in utero transplantation of cultured cynomolgus embryonic stem cells. Transplantation 2005;79:32–37.

14 Wang L, Li L, Shojaei F et al. Endothelial and hematopoietic cell fate of human embryonic stem cells originates from primitive endothelium with hemangioblastic properties. Immunity 2004;21:31–41.

15 Flake AW, Harrison MR, Adzick NS et al. Transplantation of fetal hematopoietic stem cells in utero: The creation of hematopoietic chimeras. Science 1986;233:776–778.

16 Takeuchi M, Sekiguchi T, Hara T et al. Cultivation of aorta-gonad-mesonephros-derived hematopoietic stem cells in the fetal liver microenvironment amplifies long-term repopulating activity and enhances engraftment to the bone marrow. Blood 2002;99:1190–1196.

17 Takada T, Suzuki Y, Kondo Y et al. Monkey embryonic stem cell lines expressing green fluorescent protein. Cell Transplant 2002;11:631–635.

18 Suemori H, Tada T, Torii R et al. Establishment of embryonic stem cell lines from cynomolgus monkey blastocysts produced by IVF or ICSI. Dev Dyn 2001;222:273–279.

19 Nakano T, Kodama H, Honjo T. Generation of lymphohematopoietic cells from embryonic stem cells in culture. Science 1994;265:1098–1101.

20 Shibata H, Hanazono Y, Ageyama N et al. Collection and analysis of hematopoietic progenitor cells from cynomolgus macaques (*Macaca fascicularis*): Assessment of cross-reacting monoclonal antibodies. Am J Primatol 2003;61:3–12.

21 Yoshino N, Ami Y, Terao K et al. Upgrading of flow cytometric analysis for absolute counts, cytokines and other antigenic molecules of cynomolgus monkeys (*Macaca fascicularis*) by using anti-human cross-reactive antibodies. Exp Anim 2000;49:97–110.

22 Yoshioka T, Ageyama N, Shibata H et al. Repair of infarcted myocardium mediated by transplanted bone marrow-derived CD34$^+$ stem cells in a nonhuman primate model. STEM CELLS 2005;23:355–364.

23 Zhang WJ, Park C, Arentson E et al. Modulation of hematopoietic and endothelial cell differentiation from mouse embryonic stem cells by different culture conditions. Blood 2005;105:111–114.

24 Vodyanik MA, Bork JA, Thomson JA et al. Human embryonic stem cell-derived CD34$^+$ cells: Efficient production in the coculture with OP9 stromal cells and analysis of lymphohematopoietic potential. Blood 2005;105:617–626.

25 Berenson RJ, Bensinger WI, Hill RS et al. Engraftment after infusion of $CD34^+$ marrow cells in patients with breast cancer or neuroblastoma. Blood 1991;77:1717–1722.

26 Donahue RE, Kirby MR, Metzger ME et al. Peripheral blood $CD34^+$ cells differ from bone marrow $CD34^+$ cells in Thy-1 expression and cell cycle status in nonhuman primates mobilized or not mobilized with granulocyte colony-stimulating factor and/or stem cell factor. Blood 1996;87:1644–1653.

27 Negrin RS, Atkinson K, Leemhuis T et al. Transplantation of highly purified $CD34^+Thy\text{-}1^+$ hematopoietic stem cells in patients with metastatic breast cancer. Biol Blood Marrow Transplant 2000;6:262–271.

28 Nishikawa SI, Nishikawa S, Hirashima M et al. Progressive lineage analysis by cell sorting and culture identifies $FLK1^+VE\text{-}cadherin^+$ cells at a diverging point of endothelial and hemopoietic lineages. Development 1998;125:1747–1757.

29 Schlaeger TM, Mikkola HK, Gekas C et al. Tie2Cre-mediated gene ablation defines the stem cell leukemia gene (SCL/tal1)-dependent window during hematopoietic stem cell development. Blood 2005;105:3871–3874.

30 D'Souza SL, Elefanty AG, Keller G. SCL/Tal-1 is essential for hematopoietic commitment of the hemangioblast but not for its development. Blood 2005;105:3862–3870.

31 Flake AW, Hendrick MH, Rice HE et al. Enhancement of human hematopoiesis by mast cell growth factor in human-sheep chimeras created by the in utero transplantation of human fetal hematopoietic cells. Exp Hematol 1995;23:252–257.

32 Hayashi S, Peranteau WH, Shaaban AF et al. Complete allogeneic hematopoietic chimerisim achieved by a combined strategy of in utero hematopoietic stem cell transplantation and postnatal donor lymphocyte infusion. Blood 2002;100:804–812.

33 Fujiki Y, Fukawa K, Kameyama K et al. Successful multilineage engraftment of human cord blood cells in pigs after in utero transplantation. Transplantation 2003;75:916–922.

34 Miyasaka M, Morris B. The ontogeny of the lymphoid system and immune responsiveness in sheep. Prog Vet Microbiol Immunol 1988;4:21–55.

35 Erdo F, Buhrle C, Blunk J et al. Host-dependent tumorigenesis of embryonic stem cell transplantation in experimental stroke. J Cereb Blood Flow Metab 2003;23:780–785.

36 Shevinsky LH, Knowles BB, Damjanov I et al. Monoclonal antibody to murine embryos defines a stage-specific embryonic antigen expressed on mouse embryos and human teratocarcinoma cells. Cell 1982;30:697–705.

37 Kannagi R, Cochran NA, Ishigami F et al. Stage-specific embryonic antigens (SSEA-3 and -4) are epitopes of a unique globo-series ganglioside isolated from human teratocarcinoma cells. EMBO J 1983;2:2355–2361.

38 Henderson JK, Draper JS, Baillie HS et al. Preimplantation human embryos and embryonic stem cells show comparable expression of stage-specific embryonic antigens. STEM CELLS 2002;20:329–337.

39 Bieberich E, Silva J, Wang G et al. Selective apoptosis of pluripotent mouse and human stem cells by novel ceramide analogues prevents teratoma formation and enriches for neural precursors in ES cell-derived neural transplants. J Cell Biol 2004;167:723–734.

Journal of Neuroscience Research 85:1752–1761 (2007)

Activated Microglia Affect the Nigro-Striatal Dopamine Neurons Differently in Neonatal and Aged Mice Treated with 1-Methyl-4-Phenyl-1,2,3,6-Tetrahydropyridine

Hirohide Sawada,[1] Ryohei Hishida,[2] Yoko Hirata,[3] Kenji Ono,[4] Hiromi Suzuki,[4] Shin-ichi Muramatsu,[2] Imaharu Nakano,[2] Toshiharu Nagatsu,[1,4] and Makoto Sawada[4]*

[1]School of Medicine, Fujita Health University, Toyoake, Japan
[2]Division of Neurology, Department of Medicine, Jichi Medical University, Shimotsuke, Japan
[3]Department of Biomolecular Science, Faculty of Engineering, Gifu University, Gifu, Japan
[4]Research Institute of Environmental Medicine, Nagoya University, Nagoya, Japan

Microglia play an important role in the inflammatory process that occurs in Parkinson's disease (PD). Activated microglia produce cytokines and neurotrophins and may have neurotoxic or neurotrophic effects. Because microglia are most proliferative and easily activated during the neonatal period, we examined the effects of neonatal microglia activated with lipopolysaccharide (LPS) on the nigro-striatal dopamine neurons in mice treated with 1-methyl-4-phenyl-1,2,3,6-tetrahydropyridine (MPTP), in comparison with activated microglia from the aged mice. By MPTP administration to neonatal mice, the number of dopamine neurons in the substantia nigra (SN) was decreased significantly, whereas that in the mice treated with LPS and MPTP was recovered to normal, along with significant microglial activation. Tyrosine hydroxylase (TH) activity, the levels of dopamine and 3,4-dihydroxyphenylacetic acid (DOPAC), and the levels of pro-inflammatory cytokines IL-1β and IL-6 in the midbrain were elevated in the neonates treated with LPS and MPTP. On the contrary, although the number of dopamine neurons in the 60-week-old mice treated with MPTP was also decreased significantly, the microglial activation by LPS treatment caused a further decrease in their number. These results suggest that the activated microglia in neonatal mice are different from those in aged mice, with the former having neurotrophic potential toward the dopamine neurons in the SN, in contrast to the neurotoxic effect of the latter.

Key words: microglia; dopamine neurons; neonatal mice; MPTP; cytokines

Microglia play important roles in the development, differentiation, and maintenance of neural cells in the brain. They also have immunologic functions and serve to remove dead cells by phagocytic activity after brain injury or neurodegeneration. Activated microglia may play neurotoxic roles by producing pro-inflammatory cytokines, nitric oxide (NO), and reactive oxygen species (ROS; Chao et al., 1992; Hunot et al., 1996; Cassarino et al., 1997; Liu et al., 1998; Kim et al., 2000; McGuire et al., 2001; Koutsilieri et al., 2002). Activated microglia may also play neuroprotective roles by producing neurotrophic components such as interleukin-10 (IL-10), transforming growth factor-β (TGF-β), plasminogen, nerve growth factor (NGF), brain-derived neurotrophic factor (BDNF), and glial cell line-derived neurotrophic factor (GDNF; Nagata et al., 1993b; Suzumura et al., 1993; Sawada et al., 1995, 1999; Elkabes et al., 1996; Miwa et al., 1997; Batchelor et al., 1999; Nakajima et al., 2001). Other cytokines produced from activated microglia, such as tumor necrosis factor-α (TNF-α), IL-1β, and IL-6, are pleiotropic, and produce either neurotoxic or neuroprotective effects (Barger et al., 1995; Liu et al., 1998; Fisher et al., 2001; Mason et al., 2001; McGuire et al., 2001; Bolin et al., 2002; Arai et al., 2004). Neurotrophic effects of microglial

Contract grant sponsor: Ministry of Health, Labor, and Welfare of Japan; Contract grant sponsor: Ministry of Education, Culture, Sports, Science, and Technology of Japan; Contract grant sponsor: Japan Health Sciences Foundation.

*Correspondence to: Dr. Makoto Sawada, PhD, Department of Brain Life Science, Research Institute of Environmental Medicine, Nagoya University, Chikusa, Nagoya, Aichi 464-8601, Japan.
E-mail: msawada@riem.nagoya-u.ac.jp

Received 15 October 2006; Revised 15 December 2006; Accepted 18 December 2006

Published online 27 April 2007 in Wiley InterScience (www.interscience.wiley.com). DOI: 10.1002/jnr.21241

activation were found in cell-culture studies (Nagata et al., 1993a; Elkabes et al., 1996; Miwa et al., 1997; Nakajima et al., 2001), and animal models of neurodegeneration (Rabchevsky et al., 1997; Suzuki et al., 2001; Hashimoto et al., 2005).

Parkinson's disease (PD) is a progressive neurodegenerative disorder of dopamine (DA) neurons in the substantia nigra (SN). One of the neurodegenerative mechanisms of PD is the neuroinflammatory process, by which increased levels of cytokines such as TNF-α (Mogi et al., 1994a), IL-1β, IL-6, epidermal growth factor, and TGF-α (Mogi et al., 1994b) are found in the nigro-striatal region. Microglial activation was reported to be neurotoxic in experimental PD models produced by 1-methyl-4-phenyl-1,2,3,6-tetrahydropyridine (MPTP; Wu et al., 2002, 2003; Furuya et al., 2004). The source of increased levels of cytokines in the PD brain and cerebrospinal fluid (CSF) is most probably activated microglia (Nagatsu and Sawada, 2005). Imamura et al. (2003) reported that MHC class II-positive microglia produced TNF-α and IL-6, and were associated actively with damaged neurons and neurites in the SN of PD patients, suggesting that activated microglia might act for neuroprotection. They also showed that in PD patients activated microglia were observed not only in the SN, where DA cell death occurs but also in the hippocampus, where there is no cell death. Imamura et al. (2005) further reported that in patients with dementia with Lewy bodies (DLB), the levels of BDNF mRNA and immunochemically detected protein were decreased significantly in the hippocampus, where cell death occurs, but that they were not decreased in the PD hippocampus. These results suggest that activated microglia in the hippocampus in PD may be neuroprotective in contrast to their neurotoxic effect in DLB patients. Very recently, Sawada et al. (2006) proved the presence of neurotrophic and neurotoxic groups of microglia in the mouse brain.

In the present study, to explore possible age differences we investigated the neuroprotective or neurotoxic effects of activated microglia on DA neurons in the SN in vivo in neonatal mice in comparison to those of the cells in aged mice. Neonatal microglia are activated M-CSF-dependently from late gestation to 2 weeks, and are most proliferative and easily activated under normal circumstances (Sawada et al., 1990; Thery et al., 1990). Microglia are activated by lipopolysaccharide (LPS), and are the major LPS-responsive cells in the brain (Lehnardt et al., 2003).

MATERIALS AND METHODS

Animals

All experiments were carried out using neonatal and aged 60-week-old male C57BL/6 mice (Charles River Laboratories, Tokyo, Japan). Neonatal mice were obtained from purchased pregnant female mice. The animals were housed in a room with a 12-hr light/12-hr dark cycle with free access to food and water. All animal procedures were in accordance with the Jichi Medical University guidelines for animal care.

MPTP Administration

MPTP-HCl and LPS were purchased from Sigma (St. Louis, MO) and dissolved in saline. Neonatal mice were pretreated with intraperitoneal (i.p.) injections of saline or LPS (1.0 mg/kg) daily for 5 days from postnatal day 3 (P3) to P7, and then injected with MPTP (20 mg/kg i.p.) daily for 5 days. Male 60-week-old mice received 5 consecutive days of saline or LPS injections, but only a single injection with MPTP (20 mg/kg) was carried out on the last day of LPS treatment; for repeated injection of LPS and MPTP was lethal in the aged mice. Control mice received only saline injections according to the same schedule. All mice were sacrificed 24 hr after the last MPTP injection.

Preparation of Brain Tissue

For histologic analysis, mice were anesthetized with sodium pentobarbital (50 mg/kg i.p.) and perfused intracardially with 2% paraformaldehyde in 0.1 M phosphate-buffer (PB). The brains were removed and postfixed in the same fixative for 6 hr at 4°C. They were washed with 10–20% sucrose/0.1 M PB for 24 hr at 4°C and thereafter quickly frozen in Tissue-Tek OCT compound embedding matrix (Sakura Finetek, Tokyo, Japan) and cut as 8-μm-thick coronal sections with a cryostat. For biochemical analysis, mice were anesthetized and perfused with 0.1 M PB, after which their brains were dissected out, frozen quickly in liquid nitrogen, and kept at −80°C.

Immunohistochemistry

Fixed brain tissues were immunostained by the double immunofluorescence method for light microscopy. Tissue sections were fully dried, then re-fixed in cold acetone for 10 min at room temperature, and washed in phosphate-buffer saline (PBS). Non-specific reactions were blocked by incubation for 1 hr at room temperature in blocking solution containing 10% normal goat serum and 1% bovine serum albumin in PBS. The sections were first incubated for 12 hr at 4°C with a blocking solution-diluted primary antibody specific for a microglial marker. They were washed with PBS and incubated with the appropriate fluorescent secondary antibody for 1 hr at room temperature. After having been washed in PBS, the sections were reacted with a second set of primary antibody against another marker and the appropriate secondary fluorescent antibody under the same conditions. For immunofluorescence staining of microglia, two monoclonal antibodies were used as primary antibodies, rat anti-CD11b (M1/70.15.11.5.2, Cell Hybridoma Bank) or rat anti-F4/80 (HB-198, Cell Hybridoma Bank). Other primary antibodies used were rabbit polyclonal anti-tyrosine hydroxylase (TH, diluted 1:5,000) (Nagatsu et al., 1977) for DA neurons, and rabbit polyclonal anti-caspase-3 (cleaved type) antibody (diluted 1:400; Cell Signaling, Beverly, MA) for apoptosis detection. The fluorophore-conjugated secondary antibodies used were goat Cy3 anti-rat IgG (diluted 1:400; Rockland, Gilbertsville, PA) and goat Alexa Fluor 488 anti-rabbit IgG (diluted 1:400; Molecular Probes, Eugene, OR). The nuclei in these sections were stained with 1 mg/ml of 4′,6-diamidino-2-phenylindole (DAPI; Dojindo, Kumamoto, Japan) for 10 min, after which

the sections were mounted with aqueous DAKO fluorescence mounting medium.

Fluoro-Jade B Staining

Degenerating neurons were detected by Fluoro-Jade B (FJB) fluorescence staining (Schmued and Hopkins, 2000). After sections had been immersed in a solution containing 1% sodium hydroxide in ethanol and washed in distilled water, they were transferred to a solution of 0.06% potassium permanganate for 10 min. Then the sections were washed and stained with 4×10^{-4}% FJB solution including 0.1% acetic acid for 20 min. They were washed with distilled water, fully dried, and mounted with non-aqueous mounting medium (Entellan neu, Merck, Whitehouse, NJ).

Quantitative Morphologic Analysis

Quantitative analysis of DA neurons and microglia in the SN were carried out by double-immunostaining for TH and CD11b or F4/80, respectively. Immunofluorescence images were captured with an imaging system (Sensys, CCD Camera; Photometrics, Tokyo, Japan) connected to a computer with an image program (IP Lab software; Signal Analytics, Palo Alto, CA). Numbers of cells were counted in every fifth 8-μm section throughout the entire SN. For counting DA (A9) neurons in the SN pars compacta (SNc), the total number of these neurons were calculated from the total number of TH positive cells throughout the entire SNc (Aguirre et al., 1999), which corresponded to the representative levels from Bregma −2.92 (Franklin and Paxinos, 1997) to Bregma −3.64 (Franklin and Paxinos, 1997). The number of microglia per section of the SNc was also counted. The total number of sections per mouse was from 8–10. Cell counting was carried out at low-power magnification (100×). The data were expressed as the mean ± SD and examined for statistical differences by using the unpaired Student's *t*-test (StatView, Cary, NC).

Assay of TH Activity and Contents of Dopamine and DOPAC

TH activity was analyzed by measuring enzymatically formed L-3,4-dihydroxyphenylalanine (DOPA; Hirata et al., 2001). The incubation mixture consisted of 0.2 M Tris-acetate (pH 6.0), 20 μg catalase, 1 mM 6-methyl-5,6,7,8-tetrahydropterin, 0.1 M 2-mercaptoethanol, 0.2 mM tyrosine, and 40 μL of homogenate as enzyme. Incubation was carried out at 37°C for 10 min in a total volume of 200 μL. The contents of DOPA, dopamine, and its metabolite, 3,4-dihydroxyphenylacetic acid (DOPAC), were determined by high-performance liquid chromatography (HPLC) with electrochemical detection (EICOM, Kyoto, Japan).

Cytokine Analysis

Analyses of cytokines were carried out by using mouse enzyme-linked immunoabsorbent assay (ELISA) systems for TNFα, IL-1β, and IL-6 (Quantikine, R&D Systems, Minneapolis, MN). This assay is based on the quantitative sandwich enzyme immunoassay with a purified antibody specific for each cytokine. Brain tissues were weighed and homogenized in 9 vol of 50 mM Tris-HCl buffer containing 5 mM EDTA, 1 mM dithiothreitol, 1 mM phenylmethylsulfonylfluoride, and 5 μg/mL leupeptin. The homogenates were then centrifuged at 15,000 × *g* for 10 min, and supernatants were used for cytokine analysis. Briefly, a 50-μL sample or standard was added to each microplate well-coated with a primary antibody. After a wash with buffer, the identical antibody conjugated to horseradish peroxidase was added, followed by tetramethylbenzidine substrate solution as chromogen. Protein concentrations were measured with a Micro BCA Protein Assay Kit (Pierce Biotechnology, Rockford, IL) using bicinchoninic acid for the detection of Cu^{+} formed from Cu^{2+} by protein.

RNA Preparation and RT-PCR

Total RNA extracted from frozen tissue samples of midbrain using a modified acid phenol-guanidine method was used as a template for first-strand cDNA synthesis as following method. A random primer (0.1 μg) was incubated at 95°C for 10 min with the RNA (1 μg) in a volume of 30 μl, and then placed on ice for 5 min. Next, this mixture was incubated at 37°C for 90 min with a mixture of 100 U M-MLV reverse transcriptase (Gibco BRL, Grand Island, MI), 1× reverse transcription buffer, 10 mM dithiothreitol, 40 U RNase inhibitor, and 0.56 mM each of dATP, dGTP, dCTP, and dTTP in a volume of 50 μl, then heated at 95°C for 10 min. The cDNA was amplified with Taq DNA polymerase (Takara, Otsu, Japan) using primer pairs specific to NGFβ (sense primer: AGTTTTACCAAGGGAGCA, antisense primer: GGCAGTGTCAAGGGAATG), BDNF (sense primer: AAGAAAGCCCTAACCAGT, antisense primer: CGAAAGTGTCAGCCAATG), neurotrophin (NT)-3 (sense primer: GCTTATCTCCGTGGCATC, antisense primer: TGTTGTCGCAGCAGTTCG), GDNF (sense primer: GCCAGAGGATTAT-CCTGA, antisense primer: CCCAGACCCAAGTCAGTG), or NT-4/5 (sense primer: GCTGTGGACTTGCGTGG, antisense primer: GCCCGCACATAGGACTG) for 35 cycles (94°C for 1 min, 55°C for 1 min, and 72°C for 2 min), and GAPDH (sense primer: GAAGGTGAAGGTCGGAGTC, antisense primer: GAAGATGGTGATGGGATTTC) for 30 cycles. The 195-bp (NGFβ), 260-bp (BDNF), 257-bp (NT-3), 240-bp (GDNF), 209-bp (NT-4/5), and 228-bp (GAPDH) PCR products were resolved by electrophoresis in 2% agarose gels, stained with ethidium bromide, and photographed.

RESULTS

Morphological Alterations of Microglia in Neonatal and Aged Mice Administered MPTP

Immunohistochemical study of the DA (A9) neurons in the SNc was carried out by using antibody against TH, and activated microglia were stained with antibody against CD11b. The number of TH-positive DA (A9) neurons in the SN was decreased in MPTP-treated (MPTP) group mice, as compared with saline-treated control (saline) group mice. However, in mice treated with LPS and MPTP (LPS-MPTP) group, the number of DA (A9) neurons was recovered from MPTP group mice (Fig. 1A). In the neonatal mice, the majority

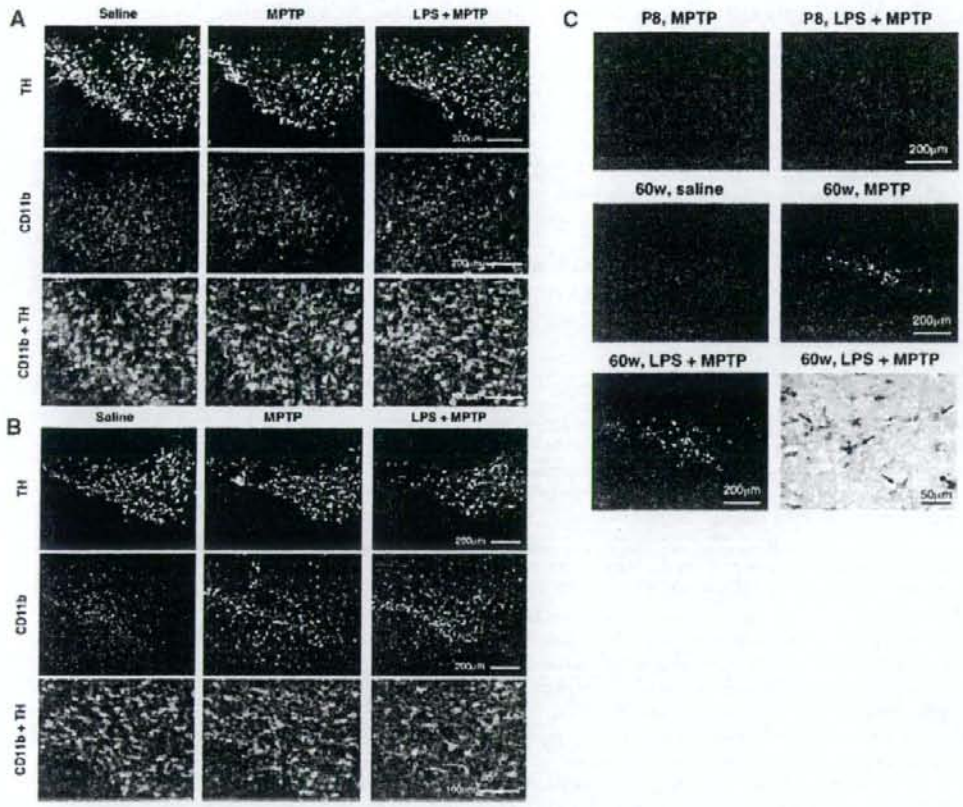

Fig. 1. Morphological changes due to MPTP administration in the SN. Immunostaining for tyrosine hydroxylase (TH)-positive dopamine (DA) (A9) neurons (merged, green) and CD 11b-positive activated microglia (merged, red) in the SN from mice treated with saline, MPTP, and LPS-MPTP are shown. **A:** In neonatal mice, DA (A9) neurons in the SN were decreased in MPTP-treated mice, whereas these neurons in the LPS-MPTP-treated mice were recovered, compared from MPTP-treated mice. The activated microglia had increased in number in the entire SN in mice treated with LPS-MPTP, as compared with saline- or MPTP-treated mice. **B:** In the aged mice, numbers of the DA (A9) neurons were decreased in the order of saline, MPTP, and LPS-MPTP treatments. In the MPTP- and LPS-MPTP-treated mice, numbers of the activated microglia were increased with their accumulation in the SNc, and the majority of the microglia showed amoeboid features. **C:** Detection of neuronal degeneration by Fluoro-Jade B (FJB) staining in MPTP-treated neonatal and aged mice. P8 refers to postnatal day 8; and 60w, to 60-week-old mice. In neonatal mice, FJB staining in the SNc of MPTP- or LPS-MPTP-treated mice were all negative. FJB staining in the SNc was negative for the aged saline-treated mice, but the MPTP- and LPS-MPTP-treated aged mice showed FJB-positive cells in their SN. Results of double staining for CD 11b-positive microglia and FJB-positive degenerative neurons in aged mice treated with LPS and MPTP are also shown. The amoeboid or ramified microglia (black) were phagocytic (arrows) or non-phagocytic (arrowheads) for FJB-positive cells (green).

of the microglia were ramified, with a small population of amoeboid ones, in the SNc or SN pars reticulata (SNr) in saline- or MPTP-treated mice. In mice treated with LPS-MPTP, activated microglia, which had thicker branched processes than resting (ramified feature) microglia, had increased in number in the entire SN (Fig. 1A). In the sections from the 60-week-old (aged) mice, the number of DA (A9) neurons was decreased in order of saline, MPTP, and LPS-MPTP groups (Fig. 1B). In the aged mice, most of the microglia were resting in the saline group, but the mice treated with MPTP and LPS-MPTP, the majority of the microglia showed amoeboid features (Fig. 1B). In both MPTP- and LPS-MPTP-treated aged mice, most of activated microglia were accumulated in the SNc, unlike the microglial distribution in the entire SN in neonatal LPS-MPTP-treated mice.

Neuronal Degeneration Due to MPTP Administration Was Observed Only in Aged Mice

DA cells in the SNc of MPTP-treated neonatal mice showed no obvious features of degeneration or cell

death as judged from the negative results of FJB staining (Fig. 1C). FJB staining of the DA (A9) neurons was negative for all of the 60-week-old of saline control mice. However, 2 of 5 MPTP-treated mice and all of the LPS-MPTP-treated mice ($n = 3$) were FJB-positive (Fig. 1C). The MPTP and LPS-MPTP groups of aged mice showed FJB-positive cells in their SN, and some of the activated microglia had phagocytosed degenerating FJB-positive cells (Fig. 1C). Cleaved caspase-3-positive DA (A9) neurons or microglia were not observed in the SN both in the neonatal and aged mice (data not shown).

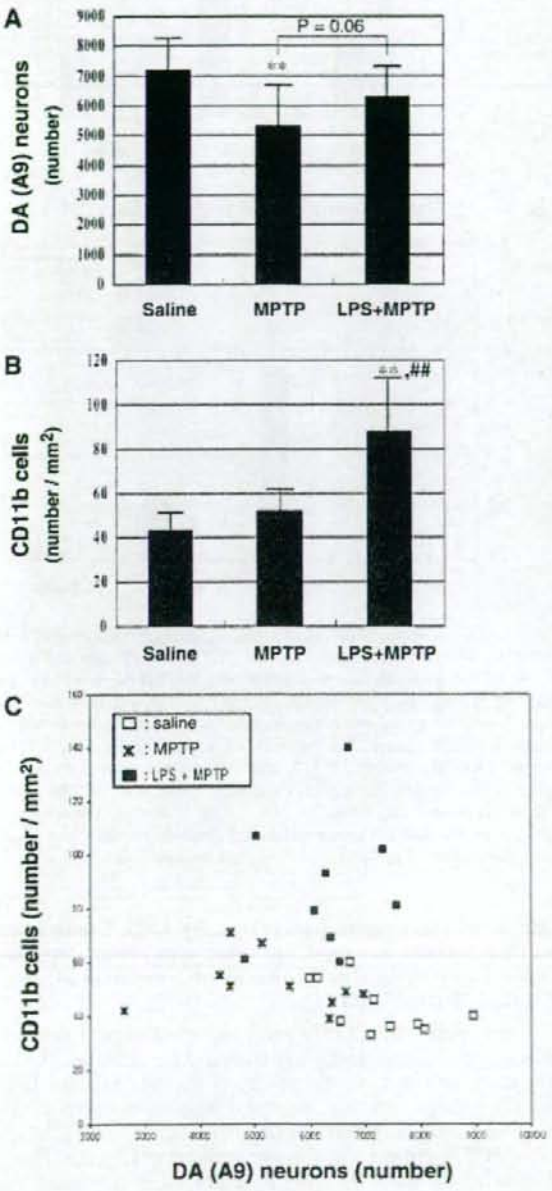

Microglial Activation by LPS Treatment Induces Neurotrophic Effects on Dopamine Cell Bodies in Neonatal Mice Administered MPTP

By MPTP administration, the number of TH-positive DA (A9) neurons in the SN of neonatal mice was significantly decreased (74% of the number for the saline group). In contrast, the number of DA (A9) neurons in the LPS-MPTP group was recovered from MPTP group (118% of the number for the MPTP group, $P = 0.06$) (Fig. 2A). The CD11b-positive microglia in the SN were increased markedly in number in the LPS-MPTP group (Fig. 2B). By staining with F4/80, another marker of microglia, there were no significant differences in their number among the three groups (data not shown).

The relationship between microglial activation and impairment of DA (A9) neurons in the MPTP-treated neonatal mice is shown in Figure 2C. A modest activation of microglia and a significant decrease in the number of DA (A9) neurons were observed in the MPTP group, whereas the LPS-MPTP group showed marked microglial activation and a tendency toward protection against cell toxicity, as compared with the MPTP group (Fig. 2C).

Effects of Microglial Activation on TH Activity and Levels of Dopamine and DOPAC in the Midbrain of Neonatal Mice Treated With MPTP and LPS

TH enzymatic activity and the contents of DA and its metabolite DOPAC in the three groups of neonatal mice were measured. In the LPS-MPTP group, TH activity was increased by 229% and 231% as compared to that of the saline group and the MPTP group, respectively (Fig. 3A). The contents of DA and DOPAC were

Fig. 2. Analysis of effects of LPS treatment on numbers of DA (A9) neurons and CD 11b-positive activated microglia in MPTP-treated neonatal mice. **A:** The number of DA (A9) neurons in the SN for the saline, MPTP, and LPS-MPTP groups is shown. The number of DA (A9) neurons in the MPTP group was decreased significantly, whereas that for the LPS-MPTP group was recovered. **B:** The number of CD11b-immunopositive microglial cells in the SN is shown. The LPS-MPTP group showed marked microglial activation. Values represent the mean ± SD. $^{**}P < 0.01$ vs. saline group; $^{\#\#}P < 0.01$ vs. MPTP group, by use of the unpaired Student's *t*-test ($n = 9$–10). **C:** Relationship between activated microglia and DA (A9) neurons in saline, MPTP, and LPS-MPTP groups of neonatal mice. Only slight activation of microglia and decrease in number of DA (A9) neurons were found for the MPTP group, whereas the LPS-MPTP group showed marked microglial activation and a tendency toward protection against loss of DA (A9) neurons compared to the MPTP group.

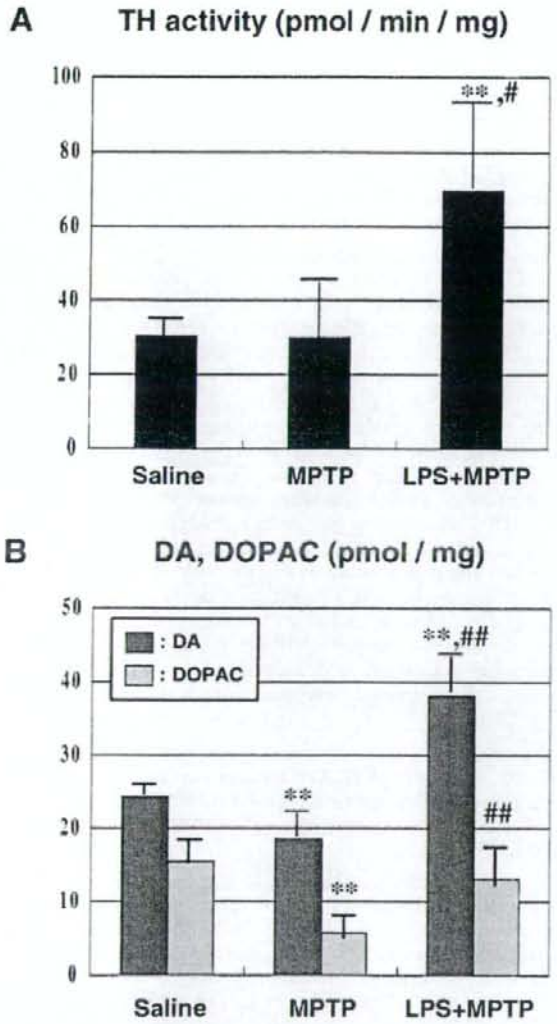

Fig. 3. Biochemical analyses of TH activity and DA and DOPAC contents in MPTP-treated neonatal mice. **A:** TH activity was measured in each of the three groups, and the LPS-MPTP group showed increased activity in the midbrain compared with the other two groups. **B:** Contents of DA and DOPAC in the midbrain after MPTP administration. Both DA and DOPAC contents were significant decreased in the MPTP group, but increased in the LPS-MPTP group. Values represent the mean ± SD. $^{**}P < 0.01$ vs. saline group, and $^{\#}P < 0.05$; $^{\#\#}P < 0.01$ vs. MPTP group, by use of the unpaired Student's *t*-test ($n = 7$–10).

decreased in the MPTP group (DA, 76%, and DOPAC, 37% of the saline group, respectively), but these values for the LPS-MPTP group were significantly higher than those for the former group (DA; 205%, and DOPAC; 227% of the MPTP group, respectively) (Fig. 3B).

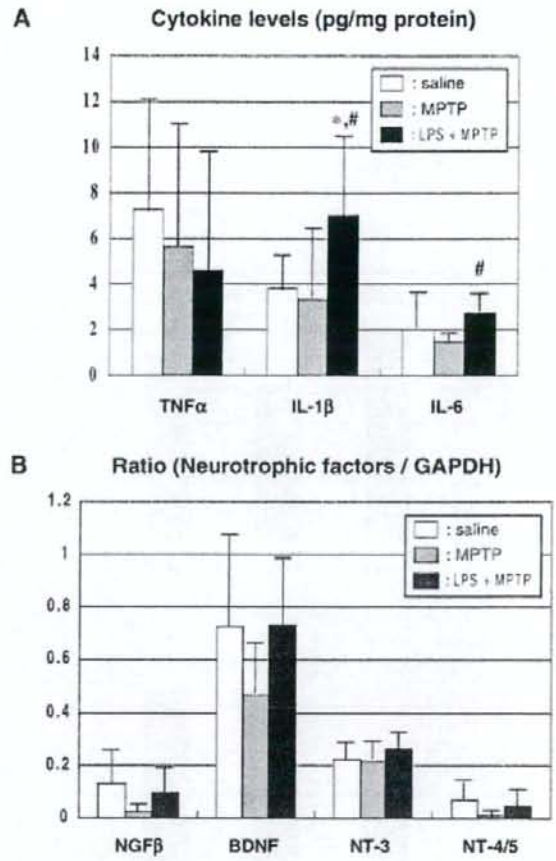

Fig. 4. Analysis of the levels of pro-inflammatory cytokines and neurotrophic factors in the midbrain of MPTP-treated neonatal mice. **A:** As to the pro-inflammatory cytokines, the TNFα level was not different among the three groups, but the IL-1β and IL-6 levels in the LPS-MPTP group were significantly higher than those in the saline and MPTP groups. **B:** The mRNA expression of neurotrophic factors, NGF-β, BDNF, NT-3, and NT-4/5 in the LPS-MPTP group were tended to higher expression than the MPTP group. Values represent the mean ± SD. $^{*}P < 0.05$ vs. saline group; $^{\#}P < 0.05$ vs. MPTP group (unpaired Student's *t*-test) ($n = 8$–9, pro-inflammatory cytokines; $n = 3$–8, neurotrophic factors).

Effects of Microglial Activation by LPS Treatment on Pro-Inflammatory Cytokines and Neurotrophic Factors Levels in the Midbrain of Neonatal Mice Treated With MPTP

By using the ELISA method, we analyzed the levels of pro-inflammatory cytokines, i.e., TNFα, IL-1β, and IL-6, in the brain tissues from the MPTP and LPS-MPTP groups. In the neonatal midbrain, the TNFα level was not different among the saline, MPTP, and LPS-MPTP groups. As shown in Figure 4A, IL-1β and IL-6 levels in the LPS-MPTP group were increased sig-